TITLE PAGE

Icotinib induces mechanism-based inactivation of rhCYP3A4/5 possibly via heme destruction by ketene intermediate

Chen Sun [#], Huimin Zhao[#], Wei Li, Yudi Jia, Yi Yang, Ying Peng, and Jiang Zheng

Wuya College of Innovation (C.S., H.Z., W.L., Y.J., Y.Y., Y.P., J.Z.), School of Pharmaceutical Engineering, Shenyang Pharmaceutical University, Shenyang, Liaoning, 110016, P.R. China; State Key Laboratory of Functions and Applications of Medicinal Plants, Guizhou Provincial Key Laboratory of Pharmaceutics (J.Z.), Guizhou Medical University, Guiyang, Guizhou, 550004, P. R. China; Key Laboratory of Environmental Pollution Monitoring and Disease Control (J.Z.), Ministry of Education, Guizhou Medical University, Guiyang, 550025, P. R. China.

RUNNING TITLE PAGE

Running Title: Mechanism-based inactivation of CYP3A by icotinib

[#]Authors contributed equally to this work.

[*]**Correspondence authors:**
Jiang Zheng, Ph.D.
Wuya College of Innovation, Shenyang Pharmaceutical University, Shenyang, Liaoning, 110016, P. R. China;
State Key Laboratory of Functions and Applications of Medicinal Plants, Guizhou Provincial Key Laboratory of Pharmaceutics, Guizhou Medical University, Guiyang, Guizhou, 550004, P. R. China.
Email: zhengneu@yahoo.com
Tel: +86-24-23986361
Fax: +86-24-23986510

The two corresponding units contributed equally to this work.

Ying Peng, Ph.D.
Wuya College of Innovation, Shenyang Pharmaceutical University, PO Box 21,103 Wenhua Road, Shenyang 110016, P. R. China
Email: yingpeng1999@163.com
Tel: +86-24-23986361
Fax: +86-24-23986510

The number of text pages: 55
The number of tables: 1
The number of figures: 11
The number of references: 41
The number of words in the Abstract: 185
The number of words in the Introduction: 589
The number of words in the Discussion: 1394

Abbreviations
BBA, 4-bromobenzylamine; CYP, cytochrome P450 enzyme; DDIs, drug-drug interactions; DTT, DL-dithiothreitol; EGFR-TKI, epidermal growth factor receptor tyrosine kinase inhibitor; EPI, enhanced product ion; GSH, glutathione; HLMs, human liver microsomes; ICT, icotinib; IS, internal standard; LLOQ, lower limit of quantitation; LOD, limit of detection; LOQ, limit of quantitation; MBI, mechanism-based inactivation; *m*-CPBA, *m*-chloroperbenzoic acid; MRM, multiple reaction monitoring; MWCO, molecular weight cut-off; NAC, *N*-acetylcysteine; NADPH, reduced nicotinamide adenine dinucleotide phosphate; NAL, *N*-acetyl lysine; NSCLC, non-small cell lung cancer; PBS, phosphate buffer solution; Pd-$BaSO_4$, palladium on barium sulfate; Pd-C, palladium on activated charcoal; PI, precursor ion; QC, quality control; r, correlation coefficient; RE, relative error; rhCYP3A4/5,

recombinant human cytochrome P450 3A4 and 3A5; ROS, reactive oxygen species; RSD, relative standard deviation; SD, standard deviation; SDS-PAGE, sodium dodecyl sulfate polyacrylamide gel electrophoresis; S/N, signal noise ratio; SOD, superoxide dismutase; TFA, trifluoroacetic acid; t_R, retention time.

Abstract

Icotinib (ICT) is an anti-tumor drug approved by China National Medical Products Administration and is found to be effective to conquer non-small cell lung cancer. The present study aimed at the interaction of ICT with CYP3A. ICT exhibited time-, concentration- and NADPH-dependent inhibitory effect on recombinant human CYP3A4/5 (rhCYP3A4/5). About 60% of CYP3A activity was suppressed by ICT at 50 μM after 30 min. The observed enzyme inhibition could not be recovered by dialysis. Nifedipine protected CYP3A from the inactivation by ICT. The inhibitory effects of ICT on CYP3A were neither influenced by GSH/NAL nor by SOD/catalase. Incubation of ICT with human hepatic microsomes produced a ketene reactive intermediate trapped by 4-bromobenzylamine. CYP3A4 dominated the metabolic activation of ICT to the ketene intermediate. Ethyl and vinyl analogs of ICT did not induce inactivation of rhCYP3A4/5, which indicates that acetylenic bioactivation of ICT contributed to the enzyme inactivation. Moreover, the metabolic activation of ICT resulted in heme destruction. In conclusion, this study demonstrated that ICT was a mechanism-based inactivator of rhCYP3A4/5, and heme destruction by the ketene metabolite may be responsible for the observed CYP3A inactivation.

Significance Statement

Cytochrome P450 enzymes play an important role in drug-drug interactions. The present study demonstrated icotinib (ICT), an inhibitor of epidermal growth factor receptor (EGFR) for the treatment of non-small cell lung cancer, is a mechanism-based inactivator of rhCYP3A4/5. The study provided solid evidence for the involvement of acetylene moiety in the metabolic activation as well as the inactivation of the enzyme. Furthermore, the resulting ketene intermediate was found to destruct heme, which is possibly responsible for the observed enzyme inactivation.

Introduction

Icotinib (ICT, **1**, Figure 1) is found to inhibit epidermal growth factor receptor (EGFR) tyrosine kinases (Tan et al., 2012). The progression and apoptosis of tumor cells are reportedly associated with the activity of the tyrosine kinases. These enzymes are often used as anti-tumor targets for drug development (Ciardiello et al., 2001). Over the decade, the U.S. Food and Drug Administration has approved several inhibitors of the kinases as anti-tumor agents against non-small cell lung cancer (NSCLC), such as afatinib, erlotinib, and gefitinib (Campbell et al., 2010; Keating et al., 2014; Gridelli et al., 2010). ICT, discovered by Betta Pharmaceuticals Co., Ltd. in China, showed favorable efficacy against NSCLC, compared with gefitinib in clinical studies (Ou et al., 2012; Shi et al., 2013; Gu et al., 2013). In 2011, ICT has been granted for the treatment of NSCLC by China National Medical Products Administration.

ICT is extensively metabolized by CYPs1A2, 2C19 and 3A4 in human liver, and CYP3A4 (53.48%) mainly contributes to the metabolism of ICT (Chen et al., 2015; Ruan et al., 2012). It is noticeable, however, that NSCLC patients administered with ICT are often treated with other drugs, due to miscellaneous conditions of clinical therapy. For instance, the regimen of ICT in combination with zoledronic acid is used for the treatment of NSCLC with bone metastases (Wang et al., 2017). ICT is combined with rapamycin for the treatment of advanced NSCLC following kidney transplantation (Zhao et al., 2014). Furthermore, ICT is often utilized together with traditional Chinese medicines in China (Zhao et al., 2017; Wu et al., 2017). These

combination therapeutic approaches may result in severe drug-drug interactions (DDIs) often found to result from inhibition of drug metabolizing enzymes, particularly cytochrome P450 enzymes (Yamreudeewong et al., 2003).

In the development of pharmaceutical agents, the ability of drug candidates to inhibit P450s needs to be examined for evaluation of DDI potential (Bjornsson et al., 2003; Obach et al., 2005). There are two types of P450 inhibition mechanisms: (I) reversible inhibition and (II) irreversible inhibition. The latter includes affinity labeling and mechanism-based inactivation (MBI). The biochemical basis for MBI generally involves metabolic activation of chemicals to reactive intermediates which are often electrophiles. Compared with the reversible inhibition, MBI may cause severe clinical safety problems because the generated reactive intermediates can irreversibly inactivate host enzymes via covalent binding of enzyme functional apoprotein or heme (Orr et al., 2012; Hollenberg et al., 2008).

ICT possesses a phenyl terminal acetylene moiety as a hydrophobic group responsible for the recognition of critical amino acids of EGFR (Stamos et al., 2002). Metabolite identification studies demonstrated that the phenyl terminal acetylene of ICT can be oxidized to the corresponding aryl carboxylic acid (Liu et al., 2011). 7-Ethynylcoumarin, *tert*-butyl acetylene and 17α-ethynylestradiol were reported to inactivate CYPs2B1, 2E1 and 3A4, respectively (Lin et al., 2002; Blobaum et al., 2002; Regal et al., 2000). These previous studies and structural characteristics made us to propose that ICT may be biotransformed to electrophilic metabolites which irreversibly inhibit P450s by modification of the host enzyme.

Time-dependent inhibitory effect of ICT on CYP3A was examined, and the nature of CYP3A inactivation by ICT was determined, according to the criteria for characterization of MBI (Silverman, 1995). The criteria for P450 MBI mainly include 1) time-, concentration- and NADPH-dependent inhibition; 2) irreversible inhibition; and 3) substrate/competitive inhibitor protection against the time-dependent inhibition. 4-Bromobenzylamine (BBA) capture experiments were also performed to identify potential ketene intermediate of ICT generated. Moreover, we investigated the correlation between the formation of ketene intermediate, heme destruction, and CYP3A inactivation.

DMD Fast Forward. Published on July 26, 2021 as DOI: 10.1124/dmd.121.000369
This article has not been copyedited and formatted. The final version may differ from this version.

Materials and Methods

Chemicals and Materials. Icotinib (ICT, ≥ 98%) was provided by Shanghai Ying-Rui- Biopharma Co., Ltd (Shanghai, China). 6β-Hydroxytestosterone was purchased from Chengdu De-Si-Te Biological Technology Co., Ltd (Chengdu, China). Palladium on barium sulfate (10% Pd-$BaSO_4$) and palladium on activated charcoal (10% Pd-C) were obtained from Wuhan Zhong-Hua-Yong-Ye Chemical Co., Ltd. (Wuhan, China). 4-Bromobenzylamine was purchased from Beijing Da-Tian-Feng-Tuo Chemical Co., Ltd. (Beijing, China). *m*-Chloroperbenzoic acid (*m*-CPBA) was acquired from Shandong Xiao-Ye Chemical Co., Ltd. (Shandong, China). Quinoline was purchased from Energy Chemical Co., Ltd. (Shanghai, China). Nifedipine and hemin were provided by Dalian Mei-Lun Biotech Co., Ltd. (Dalian, China). Testosterone, propranolol, chrysophanol, *N*-acetyllysine, glutathione, superoxide dismutase, catalase and reduced nicotinamide adenine dinucleotide phosphate (NADPH) were acquired from SolarBio Life Sciences Co., Ltd. (Beijing, China). Iodoacetamide, DL-dithiothreitol (DTT), formic acid, trifluoroacetic acid (TFA) and NH_4HCO_3 were acquired from Sigma-Aldrich (St. Louis, MO). Mixed male human liver microsomes (HLMs, donor information is listed in Supplemental Table 1) and recombinant P450 enzymes were purchased from Research Institute for Liver Diseases (Shanghai) Co., Ltd. (Shanghai, China). Trypsin and chymotrypsin (sequencing grade) were acquired from Promega Corp. (Madison, WI). BCA protein assay kits were purchased from Beyotime Biotechnology Co., Ltd (Shanghai, China). Organic solvents were obtained from Merck Life Science Co., Ltd. (Shanghai, China).

Synthesis.

N-(3-Ethylphenyl)-7,8,10,11,13,14-hexahydro-[1,4,7,10]tetraoxacyclododecino[2,3-g]quinazolin-4-amine (**Analog 2).** Synthesis of **2** (Figure 1) was conducted by catalytic hydrogenation of ICT. ICT (90 mg, 0.23 mmol) dissolved in 10 mL methanol was mixed with Pd-C (50 mg) in a hydrogen-purged flask. The mixture was stirred for 2.5 h at room temperature and then submitted to a silica gel column eluted with a mixture of CH_2Cl_2 and methanol (20:1, *v*/*v*) offering 85 mg (95% in yield) of **2** (while solid). The product was characterized by ^{1}H-NMR, MS/MS and HPLC-UV (Supplemental Figure 1 and Figure 2). MS (ESI) of $C_{22}H_{25}N_3O_4$: *m/z* 396.1 $[M + H]^+$. HPLC purity: t_R = 5.44 min (97.9%). ^{1}H-NMR (600 MHz, DMSO-d_6): δ9.41 (s, 1H), 8.47 (s, 1H), 8.15 (s, 1H), 7.61 (s, 1H), 7.31 (s, 1H), 6.96-7.73 (m, 3H), 4.29-4.31 (m, 4H), 3.76-3.80 (m, 4H), 3.64 (m, 4H), 2.62-2.65 (m, 4H), 1.21-1.24 (t, 3H).

N-(3-Vinylphenyl)-7,8,10,11,13,14-hexahydro-[1,4,7,10]tetraoxacyclododecino[2,3-g] quinazolin-4-amine (**Analog 3).** Similar procedure was followed as above for the preparation of **3** (Figure 1), except for the employment of Pd-$BaSO_4$ (20 mg) in place of Pd-C. Moreover, the activity of the reaction was quenched by adding quinoline (0.5 mL). After 1.5 h reaction, the resulting mixture was submitted to a silica gel column for purification which offered 37 mg of **3** (41% yield, white solid), followed by characterization using ^{1}H-NMR and MS/MS (Supplemental Figures 3 and 4). MS (ESI) of $C_{22}H_{23}N_3O_4$: *m/z* 394.1 $[M + H]^+$. HPLC purity: t_R = 4.47 min (96.5%). ^{1}H-NMR (600 MHz, DMSO-d_6): δ9.60 (s, 1H), 8.48 (s, 1H), 8.22 (s, 1H), 7.90 (s, 1H), 7.23 (s, 1H), 7.21-7.83 (m, 3H), 6.73-6.76 (dd, 1H), 5.82-5.85 (d, 1H), 5.28-5.30 (d,

1H), 4.29-4.30 (m, 4H), 3.74-3.79 (m, 4H), 3.63 (m, 4H).

N-(4-Bromobenzyl)-2-(3-((7,8,10,11,13,14-hexahydro-[1,4,7,10]tetraoxacyclododecino[2,3-g]quinazolin-4-yl)amino)phenyl)acetamide (ICT-BBA Adduct, **5**, Figure 5)**.** As the initial step, the terminal acetylene was oxidized by *m*-chloroperbenzoic acid (*m*-CPBA), according to a reported method (McDonald et al., 1964), and the resulting product generated *in situ* reacted with BBA. Briefly, ICT (5.0 mg), *m*-CPBA (50 mg) and BBA (25 mg) were dissolved in 10 mL CH_2Cl_2, stirred at 25 °C for 12 h, concentrated under a nitrogen stream, reconstituted in 10% acetonitrile in water, and analyzed by LC-MS/MS.

Testosterone 6β-hydroxylation assay. Reactions were composed of primary and secondary incubations. The primary mixture contained ICT (0 or 50 μM), HLMs (0.5 mg protein/mL), and $MgCl_2$ (3.2 mM) in 200 μL phosphate buffer solution (PBS, 100 mM, pH 7.4) with 0.5% organic solvent. The primary mixture was preincubated at 37 °C for 3 min, followed by adding NADPH (1.0 mM) to launch the reaction. The mixture was incubated for 0, 10, 20 or 30 min, withdrawn (40 μL), and mixed with the secondary incubation solution. The secondary incubation mixture contained $MgCl_2$ (3.2 mM), testosterone (200 μM), and NADPH (1.0 mM) in 120 μL PBS. After 15 min incubation, ice-cold acetonitrile (equal volume) was incorporated to terminate the reaction. The precipitation reagent contained propranolol (500 ng/mL) as internal standard. The supernatants were submitted to LC-MS/MS for analysis of 6β-hydroxytestosterone and propranolol after centrifugation at 19,000 *g* for 10 min.

DMD Fast Forward. Published on July 26, 2021 as DOI: 10.1124/dmd.121.000369
This article has not been copyedited and formatted. The final version may differ from this version.

To evaluate the feasibility of the method, selectivity, limit of detection (LOD), limit of quantitation (LOQ), linearity, precision, accuracy, matrix effect and stability were determined and inspired by previous literature (Foo et al., 2015). An aliquot (40 μL) of analysis solutions containing 6β-hydroxytestosterone (concentrations: 0.3, 0.75, 1.5, 3.0, 4.5, and 6.0 μg/mL) freshly prepared in methanol from a stock solution (1.0 mg/mL in methanol) was mixed with the pre-prepared incubation solution (120 μL) excluding testosterone, boiled HLMs or NADPH. The resulting mixtures were handled using the same protocol as described above (final concentrations for LC-MS/MS analysis: 10, 25, 50, 100, 150, and 200 ng/mL). The stability of analytes was determined under two storage conditions (25 °C in 12 h and -4 °C in 48 h) based on the needs of the experiments.

Determination of Time-, Concentration-, and NADPH-Dependent Inhibition of CYP3A by ICT. The primarym mixture contained HLMs (0.5 mg protein/mL), $MgCl_2$ (3.2 mM), and ICT at concentrations of 0, 5, 15, 25, 35, or 50 μM in 200 μL PBS. The mixture was preincubated for 3 min at 37 °C, followed by adding NADPH (1.0 mM) to launch the reactions. In a separate experiment, the incubation reaction received the same volume of PBS in place of NADPH to determine NADPH dependency of the enzyme inhibition. The mixture was incubated for 0, 10, 20 and 30 min, withdrawn (40 μL), and mixed with the secondary incubation solution. The secondary incubation mixture contained $MgCl_2$ (3.2 mM), NADPH (1.0 mM), and testosterone (200 μM) in 120 μL PBS. After 15 min incubation, ice-cold acetonitrile (equal volume) containing propranolol (500 ng/mL, IS) was incorporated to terminate

the reaction. Samples were then prepared and analyzed as stated above.

Examination of Effect of Substrate Protection. The primary incubation mixture contained ICT (50 μM), nifedipine (100 μM, a substrate of CYP3A), HLMs (0.5 mg protein/mL), and $MgCl_2$ (3.2 mM) in 200 μL PBS. The reaction was launched by incorporation of NADPH (1.0 mM). The mixture was incubated for 0, 10, 20 and 30 min, withdrawn (40 μL), and mixed with the secondary incubation solution. The contents of the secondary incubation mixture and sample preparation for analysis were the same as described above. The primary incubations which lacked ICT or/and nifedipine were conducted as the corresponding control groups.

Examination of Effects of NAL/GSH or SOD/Catalase on Inhibition of CYP3A. The primary incubation contained ICT (50 μM), HLMs (0.5 mg protein/mL), GSH/NAL (2.0 mM for each) or SOD/catalase (800 unit/mL for each), and $MgCl_2$ (3.2 mM) in 200 μL PBS. The reactions were launched by spiking with NADPH (1.0 mM), followed by incubating for 0, 10, 20 and 30 min. The resulting mixtures (40 μL) were withdrawn and mixed with the secondary incubation solution. The content of the secondary incubation mixture and sample preparation for analysis were the same as described above.

Determination of Partition Ratio. The primary incubation included recombinant human CYP3A4 or CYP3A5 (100 nM for each), ICT (0, 3.125, 6.25, 12.5, 25, 50, 75, 100, or 200 μM), and $MgCl_2$ (3.2 mM) in 100 μL PBS. The reactions were launched by spiking with NADPH (1.0 mM). After 0 or 30 min incubation, a 40 μL aliquot of

the primary incubation solution was mixed with the secondary incubation solution. The content of the secondary incubation and sample preparation for analysis were similar as stated above.

Determination of Inhibition Reversibility. The primary incubation mixture contained ICT (50 μM), HLMs (0.5 mg protein/mL), and $MgCl_2$ (3.2 mM) in 200 μL PBS. The reaction was launched with NADPH (1.0 mM). After 0 or 30 min incubation, the vehicle- and ICT-treated samples were dialyzed (MWCO: 3,500 Da) in a PBS solution (1 L) at 4 °C. The buffer was changed every two hours for three times. In parallel, the non-dialyzed control and inactivation samples were stored under the same cool condition during the dialysis process. All samples were mixed with the secondary incubation mixture. The content of the secondary incubation and sample preparation for analysis were the same as described above.

CYP3A Activity Assessment. The remaining enzyme activitity of CYP3A was assessed by monitoring the formation of metabolite 6β-hydroxytestosterone from probe substrate testosterone by LC-MS/MS. An Agilent 1260 HPLC system (Agilent Technologies, Santa Clara, CA) inlined with an AB 5500 triple quadrupole mass spectrometry (SCIEX, Foster City, CA) was used for metabolite assessment. Metabolite responsible for CYP3A (*m/z* 305→269) was assessed by LC-MS/MS in a positive mode, and propranolol (*m/z* 261→116) was selected as internal standard in a positive mode, respectively. Chromatographic separation was achieved on a ZORBAX C_{18} column (5.0 μm, 150 mm × 4.6 mm; Agilent Technologies, Santa Clara,

CA) eluted with mobile phases consisting of acetonitrile and water which contain 0.1% formic acid. The gradient parameters for the determination of the metabolite related with CYP3A are listed in Supplemental Table 2, respectively.

Ketene Reactive Intermediate Trapping by 4-Bromobenzylamine (BBA). A microsomal incubation mixture contained ICT (50 μM), HLMs (0.5 mg protein/mL), BBA (trapping agent, 5.0 mM), and $MgCl_2$ (3.2 mM) in 200 μL PBS. NADPH (final concentration: 1.0 mM) was spiked to launch the reaction while control group lacked NADPH. After 30 min incubation at 37 °C, ice-cold acetonitrile (equal volume) was incorporated to terminate the reaction, followed by centrifugation at 19,000 *g* for 10 min. The resulting supernatants were subjected to analysis by LC-MS/MS. The formation of ICT-BBA adducts was monitored by scanning of precursor ion (PI) *m/z* 169 and 171 as well as ion pairs *m/z* 593→479 and 595→481 in a positive mode. In addition, tandem mass spectra of the detected adducts were acquired in an enhanced product ion (EPI) mode. HPLC separation was achieved on the ZORBAX C_{18} column eluted with a mobile system consisting of acetonitrile and water with 0.1% formic acid. The protocol for gradient elution is shown in Supplemental Table 3.

Comparison of Inactivation Effect of ICT, 2 and 3 on CYP3A. The primary incubation mixture contained ICT, **2** or **3** (50 μM for each), HLMs (0.5 mg protein/mL), and $MgCl_2$ (3.2 mM) in 200 μL PBS. NADPH (1.0 mM) was incorporated to launch the reaction. Control group received vehicle instead of ICT, **2** or **3**. The primary mixture was incubated at 37 °C for 0, 10, 20 or 30 min, followed by mixing (40 μL aliquots) with the secondary incubation mixture. The content of the secondary incubation mixture and sample preparation for analysis were the same as described above.

Recombinant Human P450 Incubations. ICT (50 μM), NADPH (1.0 mM) and individual recombinant human P450 enzymes, such as CYPs3A5, 3A4, 2E1, 2D6, 2C19, 2C9, 2B6, 2A6 and 1A2, (100 nM) were mixed and incubated at 37 °C for 30 min. The reaction was stopped by ice-cold acetonitrile (equal volume) which contains propranolol (500 ng/mL, IS).

Determination of Heme Damage. A recombinant enzyme incubation mixture contained ICT (50 μM), CYP3A4 (100 nM), and $MgCl_2$ (3.2 mM) in 100 μL PBS. To launch the reaction, the incubation mixture received NADPH at final concentration of 1.0 mM, while control incubation lacked NADPH. After incubating at 37 °C for 30 min, the resulting mixture was extracted with ten volumes of butanone containing 0.1% TFA and 2.5 ng/mL propranolol (IS). The resulting organic phase was concentrated by blowing with N_2 to dryness, and re-constituted in methanol (200 μL). After filtration through a 0.22 μm membrane, the resulting filtrates were analyzed by LC-MS/MS. Detection of heme and propranolol was achieved by monitoring *m*/*z* 616→557 and 260→116 in a positive ion mode. HPLC separation was performed on the ZORBAX C_{18} column. The column was eluted with water and methanol which contain 0.1% formic acid as shown in Supplemental Table 4. Tandem mass spectrum of heme was acquired in a mode of EPI.

Proteomic Analysis of CYP3A4 Apoprotein after Exposure to ICT. Inactivation of CYP3A4 by ICT (50 μM) was performed as described above. The resulting inactivated recombinant CYP3A4 was dialyzed (MWCO: 3,500 Da) at 4 °C in PBS buffer (1 L, 100 mM, pH 7.4) for 6 h (2 h × 3). Protein contents were assessed by a BCA protein assay kit. The protein samples were separated on SDS-PAGE (15%), according to the general procedure. After 1 h discoloring and rehydrating at 60 °C

in a 50 mM ammonium bicarbonate solution containing 10 mM DTT, the gel responsible for CYP3A4 was sliced and discolored with 50% acetonitrile in a 50 mM NH_4HCO_3 solution for approximately 30 min to make sure micelles colorless. The resulting micelles were placed in 100 μL acetonitrile and allowed to stand at 25 °C for 30 min. The resulting aggregated micelles were mixed with 10 mM DTT dissolved in a 50 mM NH_4HCO_3 solution (100 μL) and stirred at 56 °C for 1 h. The resultant incubation was mixed with 50 mM iodoacetamide dissolved in 50 mM NH_4HCO_3 (100 μL) and was allowed to stand at 25 °C in dark for 60 min. The resultant micelles were placed in 100 μL acetonitrile, allowed to stand for 30 min, and incubated with trypsin (15 ng/μL) in 50 mM NH_4HCO_3 or chymotrypsin (25 ng/μL) in 10 μL Tris-HCl (pH 8.0, 100 mM) digestion solution at 37 °C for 16 h. The resultant micelles were mixed with 50% acetonitrile in water (100 μL) containing 5% TFA, placed at 37 °C for 1 h for peptide extraction, and lyophilized to near dryness, followed by mixing with 10 μL 0.1% formic acid and LC-MS/MS analysis. Sample analyses were conducted on a Q Exactive Hybrid Quadrupole-Orbitrap Mass Spectrometer (Thermo Fisher Scientific, San Jose, CA) interfaced with an Ultimate 3000 Nanoflow UPLC System (ThermoFisher Scientific, San Jose, CA). Analyte separation was achieved on a ReproSil-Pur C_{18}-AQ resin column (1.9 μm, 150 μm × 15 cm, 100 Å) provided by Dr. Maisch (Ammerbuch, Germany). The column was eluted with water and acetonitrile which contain 0.1% formic acid. The gradient protocol for eluting of the peptides is shown in Supplemental Table 5. The analysis of raw MS files and target protein identification were achieved via searching target protein database by accessing to Maxquant (1.6.2.10).

Statistical Analysis. All of the data reported represent the mean ± standard deviation (SD). All quantitative experiments were independently repeated three

times, and the results were averaged.

Results

Methodology Validation. Incubation mixtures containing boiled microsomes in the absence of 6β-hydroxytestosterone and the IS were analyzed by LC/MS/MS. No peaks responsible for *m*/*z* 305→269 and 261→116 were observed (Supplemental Figure 5), indicating that no matrix interference was involved and that the analysis was highly selective. The LOD and LOQ of 6β-hydroxytestosterone were found to be 2.5 ng/mL (S/N = 3.9) and 10 ng/mL, respectively. A six-point calibration curve (final concentration range: 10-200 ng/mL) was established and assessed with correlation coefficient (r) of ≥ 0.99, precision of ± 15%, and accuracy of ± 15%, which is all acceptable. Samples containing 6β-hydroxytestosterone at concentrations of 12.5 (low), 75.0 (medium) or 175 ng/mL (high) for the determination of lower limit of quantitation (LLOQ, 10 ng/mL) and quality control (QC), the intra-day (n = 6) and inter-day (n = 3) RSD values of the analyte were less than 12.8%, and the accuracy was 91.5%-111.1% of the nominal value, indicating that the LC-MS/MS method is reliable and reproducible. The matrix effect obtained from comparison of samples containing boiled HLMs with that lacking boiled HLMs, ranged from 98.2% to 103.6% in QC samples (n = 6). Clearly, no significant matrix effect was observed in response to 6β-hydroxytestosterone. Moreover, we examined the stability of the incubation mixtures under the various storage conditions that may be applied to the experiments. Samples were stable at 25 °C in 12 h and 4 °C in 48 h. All methodological data are shown in Supplemental Table 6.

Screening of Time-Dependent Inhibition of CYP3A by ICT. ICT (0 and 50 μM)

was incubated with human hepatic microsomes, followed by examining the remaining activitity of CYP3A. Incubation of human liver microsomes with ICT at 50 μM for 30 min resulted in a significant loss (> 50%) of CYP3A activity Supplemental Figure 6). Therefore, it leads us to speculating that ICT may be a MBI of CYP3A.

Time-, Concentration-, and NADPH-Dependent Inhibition of CYP3A by ICT. Comprehensive enzymatic kinetics were performed to examine time-, concentration-, and NADPH dependency of ICT-induced CYP3A inhibition. Determination of 6β-hydroxytestosterone formed in the secondary incubation fortified with testosterone was carried out to assess the resulting CYP3A activity remained. The remaining enzyme activity of the incubation mixture of each concentration at 0 min was normalized to 100%. Decreased CYP3A activity was observed in microsomal incubation with ICT in a time-dependent manner (Figure 2A). Additionally, the higher ICT concentration was applied in the incubation, the faster the enzyme was inhibited. About 56% of CYP3A activity was suppressed by ICT (50 μM) after 30 min incubating at 37 °C. Kinetic constants k_{inact} and K_I were estimated using Wilson's plot established by plotting of reciprocal rates of inactivation (k_{obs}) acquired vs reciprocal ICT concentrations (Figure 2B). The values of k_{inact} and K_I were found to be 0.013 min^{-1} and 20.8 μM, respectively. In addition, ICT failed to show such time-dependent inhibition in NADPH-free incubations (Figure 2C). This suggests the involvement of metabolism in the observed CYP3A inhibition.

Substrate Protection. Nifedipine, a substrate of CYP3A, was used to evaluate substrate protection against the enzyme inactivation induced by ICT. Around 47%

DMD Fast Forward. Published on July 26, 2021 as DOI: 10.1124/dmd.121.000369
This article has not been copyedited and formatted. The final version may differ from this version.

of CYP3A activity remained after 30 min incubation with ICT alone (50 μM) at 37 °C. However, in parallel, the remaining CYP3A activity was found to be about 80% in the microsomal incubation fortified with nifedipine (Figure 3). Clearly, nifedipine slowed down the CYP3A inactivation caused by ICT, indicating that bioactivation of ICT occurred in the active site of CYP3A.

SOD/Catalase Effects on Enzyme Inactivation. P450-catalyzed reactions could produce reactive oxygen species (ROS). The resulting ROS, such as hydrogen peroxide and superoxide radical anion, could induce the inactivation of the host enzymes. Catalase and superoxide dismutase (SOD), known as ROS scavengers, were included in ICT-fortified microsomal incubations to determine possible roles of ROS in the observed CYP3A inactivation. The presence of the two ROS scavengers revealed little protective effects on ICT-induced CYP3A inactivation (Table 1). This enables us to exclude the involvement of hydrogen peroxide and/or superoxide that may lead to auto-inactivation even if ROS were formed during the metabolic process of ICT.

GSH/NAL Effects on Enzyme Inactivation. GSH and NAL were fortified in ICT microsomal incubations to determine the protection of exogenous nucleophiles against the CYP3A inactivation. It appears that the two nucleophilic agents failed to offer protection against the inactivation of CYP3A induced by ICT (Table 1). This suggests that reactive intermediates of ICT inactivated the CYP3A prior to leaving the enzyme active site.

Partition Ratio (*P* value). *P* value stands for the numbers of molecules of the metabolite required for the inactivation of the targeting enzyme. *P* value was measured to evaluate the efficiency of ICT on the inactivation of rhCYP3A4/5. The value was estimated by plotting of the percentage of residue activity vs molar ratio of ICT/CYP3A4 or ICT/CYP3A5, according to a published method (Silverman et al., 1995). ICT at the ICT/CYP3A4 molar ratio above 500 inactivated CYP3A4 about 74% (Figure 4A) and did not further inactivate the enzyme while ICT inactivated CYP3A5 about 55% (Figure 4B). Meanwhile, turnover numbers (*P* + 1) for CYP3A4 and CYP3A5 were 174 and 277, respectively. Thus *P* values were 173 and 276, respectively. Reported *P* values for MBI of P450s are in the range of 3 (highly efficient inactivators) to > 1,000 (inefficient) (Kent et al., 2001). Thus, ICT may be considered to be a moderately efficient inactivator of CYP3A.

Irreversibility of Inhibition. Irreversibility of the observed inhibition was probed by exhaustive dialysis of ICT-exposed HLMs. The remaining CYP3A activity of dialyzed sample pretreated with ICT was 39.3 ± 8.3%, while that of non-dialyzed samples was 35.5 ± 6.1%. This indicates that ICT irreversibly inhibited CYP3A and the inhibited CYP3A activity could not be recovered by dialysis.

Generation of Ketene Reactive Intermediate. We speculated ICT may be metabolized to ketene intermediate **4** (Figure 5) and then decided to trap the intermediate using 4-bromobenzylamine (BBA). The generation of the

DMD Fast Forward. Published on July 26, 2021 as DOI: 10.1124/dmd.121.000369
This article has not been copyedited and formatted. The final version may differ from this version.

corresponding adduct was determined by LC-MS/MS in MRM model (ion pairs scanned: *m/z* 593→479 and 595→481). A peak with retention time at 10.9 min was observed in ICT-fortified microsomes in the presence of NADPH (Figures 6C and 6D). We failed to detect such peak in NADPH-free incubations (Figures 6A and 6B). The observation of *m/z* 593 and 595 (molecular ions) enabled us to propose the structure of ICT-BBA adduct **5** (Figure 5). The observed representative fragments *m/z* 169, 171, 479 and 481 are possibly responsible for bromobenzyl and quinazoline phenyl portions, respectively. Fragments *m/z* 294 and 266 may arise from the loss of BBA with and without carbonyl part (Figure 6E and Figure 6F).

Biomimetic synthesis was conducted to verify the proposed structure of ICT-BBA adduct **5**. The terminal acetylene of ICT was oxidized by *m*-CPBA, reacted with BBA, and analyzed by LC-MS/MS. A product in the synthetic sample showed similar t_R (Figure 7A and Figure 7B) and MS/MS fragment patterns (Figures 7C and 7D) as that detected in microsomal incubation mixtures.

Role of Acetyleneic Moiety in Inactivation of CYP3A by ICT. ICT analogs **2** and **3** (Figure 1) were designed and synthesized to determine the functional group responsible for the metabolic activation. As expected, analogs **2** and **3** failed to show time-dependent inhibition of CYP3A (Figure 8). This indicates that the acetylenic moiety played an essential role in ICT-induced CYP3A inactivation, which further supports the proposed involvement of the ketene reactive intermediate in the inactivation of CYP3A by ICT.

P450 Enzymes Participating in Bioactivation of ICT. ICT was incubated with a selection of individual recombinant human P450 enzymes. Relative contributions of P450 enzymes to the bioactivation of ICT were determined by monitoring the production of ICT-BBA adduct **5**. Figure 9 shows the enzymes involved in the ketene intermediate formation. CYP3A4, followed by CYPs2D6 (20.9 ± 3.5% of CYP3A4) and 3A5 (12.0 ± 3.6% of CYP3A4) in order of enzyme catalysis efficacy, was the major enzyme participating in the observed bioactivation.

Changes of the Prosthetic Heme Resulting from Inactivation of CYP3A4 by ICT. Heme contents of recombinant CYP3A4 after exposure to ICT with or without NADPH were measured to determine heme destruction resulting from the metabolic activation of ICT. Internal standard propranolol (t_R = 10.39 min, Figure 10A) enabled us to correct and minimize the errors resulting from instrumental fluctuation and experimental operation. The mass spectrometry response intensity (peak area) of propranolol was consistent in incubations containing ICT and CYP3A4 without (Figure 10C) or with (Figure 10E) NADPH. Authentic hemin standard eluted at 13.62 min (Figure 10B) and the MS/MS spectrum of hemin revealed major product ions at *m*/*z* 557 and $[M\text{-}Cl]^+$ at *m*/*z* 616 (quasi-molecular ion, Figure 11). This allowed us to select the ion pair (MRM) to monitor prosthetic heme in incubation mixtures. However, decreased contents of the heme were observed in NADPH-supplemented incubations (Figure 10F), compared with that of NADPH-free incubations (Figure 10D). The peak area ratios of heme/propranolol in NADPH-free incubation fortified with ICT was defined as 100% to determine the involvement of

heme in enzyme inactivation. As shown in Figure 10, incubation of recombinant CYP3A4 with ICT at 50 μM for 30 min resulted in an approximately 82% decrease in the content of prosthetic heme.

Interaction of CYP3A4 Apoprotein with Ketene Intermediate. We also examined the modification of apoprotein by the ketene intermediate using mass spectrometry. Protein obtained from ICT-treated incubation mixture was hydrolyzed by trypsin or chymotrypsin and submitted to LC-MS/MS to determine protein modification. We failed to detect the peptides with an increased molecular weight of 407.148 Da ($C_{22}H_{21}N_3O_5$, the mass of ketene intermediate) in positive mode, even with mass tolerance set at 20 ppm (Supplemental information). Only some unmodified and oxidized peptides from CYP3A4 were detected by LC-MS/MS. This allowed us to exclude the possibility of protein modification as a mechanism for ICT-induced CYP3A inactivation.

Discussion

Our study provided, for the first time, the evidence for time-dependent inhibition of CYP3A4/5 by ICT (Figure 2), with values of k_{inact} of 0.013 min^{-1} and K_I of 20.8 μM. ICT-induced CYP3A inactivation was not observed in the incubation mixture without NADPH, indicating that the enzyme inactivation was mediated by biotransformation of P450 enzymes. Mechanism-based inactivation should lie in the metabolic activation of an inactivator precursor and sequential reaction of the host enzyme with the resulting reactive intermediate prior to leaving the binding pocket. Nifedipine, a substrate of CYP3A, slowed down the CYP3A inactivation induced by ICT (Figure 3), suggesting that the bioactivation of ICT happened in the active site of CYP3A. Moreover, catalase/SOD did not show protective effects on ICT-induced CYP3A inactivation (Table 1), which enables us to exclude the roles of reactive oxygen species, i.e. superoxide and H_2O_2 potentially generated, in the enzyme inactivation. Therefore, the reactive intermediate produced through metabolic activation may be the culprit of the observed mechanism-based inactivation (Kent et al., 2001). GSH and NAL, as nucleophilic agents, were included in incubations for capturing possible reactive electrophilic intermediates which escape from the host enzyme. The incorporation of the nucleophiles failed to reveal protection from the inactivation of CYP3A by ICT (Table 1), which suggests that the reactive metabolite of ICT inactivated the CYP3A prior to releasing from the active site of the enzyme. Meanwhile, the inhibited CYP3A activity was not recovered by dialysis, implying that covalent modification was involved in the enzyme inactivation. Taken together, all evidence points toward the inevitable conclusion that ICT is a mechanism-based inactivator of CYP3A.

CYP3A4 is the major enzyme involved in the metabolism of ICT (Chen et al.,

2015). This enzyme is known as the most abundant enzyme of P450 superfamily in humans, and at least 50% marketed drugs are metabolized by CYP3A4. According to the relevant FDA guidance document (FDA, 2020; Vieira et al., 2014), equations for basic models of time-dependent inhibition are described in Supplemental Figure 6. It has been reported that as high as about 7.5 μM of plasma C_{max} of ICT is circulated in patients given multiple doses (Liu et al., 2015), human plasma protein binding rate of ICT is around 98.5% (Tan et al., 2009), and the turnover of CYP3A4 (k_{deg}) is 0.00016 min^{-1} (Galetin et al., 2006). For icotinib, the values of $I_{max,u}$, K_{obs} and R_2 were 0.1125 μM, 0.0028 min^{-1} and 18.5, respectively, according to the calculation formula mentioned. Since $R_2 \geq 1.25$, the DDI potential of icotinib needs further investigation for a clinical DDI study with a sensitive index substrate (FDA, 2020). For example, ritonavir is known as a potent MBI of CYP3A4 (Lim et al., 2005), and the calculated R_2 is 23-26 (Vieira et al., 2014). A study showed that CYP3A remained inhibited 3 days after termination of ritonavir exposure at doses of 300-600 mg daily (Katzenmaier et al., 2011). Ritonavir has been listed as the drug that causes DDI in humans, which is proposed to occur via MBI of CYP3A (Kalgutkar et al, 2007). Like ritonavir, ICT is a MBI of CYP3A with a higher value of R_2 (≥ 1.25), which may remind us that DDI may be clinically significant, especially co-administrated with other medicines with narrow therapeutic windows.

CYP2J2 is another hepatic P450 enzyme although the content is limited. The enzyme shares similar substrates with CYP3A. We employed nifedipine to probe potential inactivation of CYP2J2 by ICT. Nifedipine is also a mixed inhibitor of

CYP2J2 (Noriaki et al., 2019). Mechanistically, a mixed inhibitor is unable to slow down mechanism-based inactivation. Apparently, nifedipine was found to reverse the observed time-dependent inhibition of "CYP3A" (possibly overlapping with CYP2J2 in human hepatic microsomes). If ICT were a mechanism-based inactivator of CYP2J2, such protection effect on the inactivation of "CYP3A" would not have taken place. This enables us to exclude the potential inactivation of CYP2J2 by ICT.

To characterize the role played by reactive intermediates in enzyme inactivation, trapping experiments were performed in human liver microsomal incubations. Trapping agents can be classified as "soft" (GSH/NAC) and "hard" (amine derivatives) nucleophiles (Pearson et al., 1969). A ketene intermediate which is defined as a "hard" electrophile might be formed via the bioactivation of terminal alkyne of ICT. We firstly employed *N*-acetyl lysine (NAL) to capture the ketene. Unfortunately, no related adduct was detected (data not shown), possibly resulting from the sensitivity limitation of mass spectrometry. Then we selected BBA, a trapping agent which introduces a bromine in the resulting adduct, for the capture study. BBA, which has been proven to be an effective trapping agent, could be easily cleaved to fragments of *m/z* 169 and 171 with intensities of 1:1, resulting from 79/81 isotopes of bromine incorporated, in mass spectrometric analysis (Wang et al., 2014). This may allow us to avoid potential false positive and BBA was successfully employed in trapping *cis*-enedials in our early study (Wang et al., 2014). This did make the mass spectrometry detect the corresponding adduct. We oxidized ICT with *m*-CPBA and reacted the resulting product with BBA to characterize the adduct. *m*-CPBA is a

widely used oxidizing agent in epoxidation reactions. The epoxidation of ICT via biomimetic synthesis using *m*-CPBA to the corresponding oxirene or/and ketene intermediates enables us to mimic the bioactivation of ICT. We speculated that the oxidation of the terminal acetylene by *m*-CPBA offers intermediate **6** (Figure 5), followed by rearrangement to ketene intermediate **4** and reaction with BBA. In other words, *m*-CPBA mimics the oxidation of the terminal acetylene of ICT catalyzed by P450s. The designed synthetic work allowed us to verify the structure of ICT-BBA adduct **5**, which facilitates the understanding of the metabolic pathway responsible for ICT bioactivation.

Incubation of ICT with the individual recombinant enzymes demonstrated that P450s, such as CYP2D6 and CYP1A2 involved in the generation of the ketene intermediate (Figure 9), were not necessarily inactivated by the resulting reactive metabolite (data not shown). The explanation for this may result from the absence of nucleophilic amino acid residues in the active site of the metabolizing enzyme. An appropriate distance between the nucleophilic amino acid residue(s) and the reactive intermediate generated *in situ* is required for covalent binding. This may determine the effectiveness of the enzyme inactivation. Additionally, it is likely that the reactive metabolite escapes from the active site without inactivating the host enzyme (Mao et al., 2018). To further probe the role of the acetylenic group of ICT in the observed CYP3A inactivation, the terminal acetylene of ICT was chemically replaced with a vinyl or ethyl group. The vinyl and ethyl analogs showed no inhibitory effects on CYP3A at all (Figure 8), indicating the requirement of the

acetylenic group for the enzyme inactivation.

In view of the fact that ICT inactivated CYP3A4 more than CYP3A5 and that CYP3A4 was mainly involved in the ketene intermediate formation, we chose CYP3A4 as the enzyme to determine the interaction of reactive metabolites of ICT with the target enzyme. We started with apoprotein adduction investigation by trypsin and chymotrypsin digestion- and LC-MS/MS-based analysis. Unfortunately, mass spectrometric analysis failed to show the evidence for apoprotein modification derived from ICT (Supplemental Data). We then decided to examine the alteration in prosthetic heme content of CYP3A4 incubations with or without exposure to ICT. A dramatic loss (82%) of prosthetic heme content was found in the incubation mixture supplemented with ICT. The observed disappearance of prosthetic heme in ICT-treated CYP3A4 incubation suggests that heme was damaged, resulting from the metabolic activation of ICT. Cytochrome *b*5 is also potentially alkylated by reactive metabolites resulting in enzyme inactivation (Osawa et al., 1989). Our incubation system did not contain such enzyme, which excludes the participation of cytochrome *b*5 modification in the observed CYP3A4 inactivation. Together, the finding of heme destruction, along with the failure to detect modified apoprotein, in ICT-treated CYP3A4 indicates that heme rather than apoprotein was the target of the electrophilic metabolite which participates in the observed enzyme inactivation.

In summary, ICT was proved to be a moderately efficient mechanism-based inactivator of rhCYP3A4/5. Heme destruction by a ketene intermediate biotransformed from the terminal acetylenic moiety of ICT may be responsible for

ICT-induced CYP3A inactivation. It alerts clinicians to be cautious about the potential risk of ICT-induced drug-drug interactions and provides the foundations for the rational design of new drug entities.

DMD Fast Forward. Published on July 26, 2021 as DOI: 10.1124/dmd.121.000369
This article has not been copyedited and formatted. The final version may differ from this version.

Supplemental Data [additional figures and data]

Donor information of mixed male human liver microsomes; Gradient elution protocol for separations of 6β-hydroxytestosterone, possible ICT-BBA adducts, heme, propranolol, and peptides; Precision, accuracy, matrix effect and stability of 6β-hydroxytestosterone; ^{1}H-NMR, HPLC-UV, and MS/MS spectra of the ethyl analog of icotinib and the vinyl analog of icotinib; Representative MRM chromatograms of 6β-hydroxytestosterone and propranolol obtained from analysis of boiled microsomal incubation mixtures lacking 6β-hydroxytestosterone and propranolol and of these spiked with 6β-hydroxytestosterone for the determination of LOD or LLOQ; Equations to calculate R_2 value for basic models of time-dependent inhibition (PDF); Peptide fragment profile of CYP3A4 by LC-MS/MS (XLSX)

Authorship contributions

Participated in research design: Sun, Zhao, Peng and Zheng.

Conducted experiments: Sun, Zhao, Li, Jia and Yang.

Performed data analysis: Sun and Zhao.

Wrote or contributed to the writing of the manuscript: Sun, Zhao and Zheng.

References

Bjornsson TD, Callaghan JT, Einolf HJ, Fischer V, Gan L, Grimm S, et al (2003) The conduct of in vitro and in vivo drug-drug interaction studies: a PhRMA perspective. *Drug Metab Dispos* **43**:443-469.

Blobaum AL, Kent UM, Alworth WL, Hollenberg PF (2002) Mechanism-based inactivation of cytochromes P450 2E1 and 2E1 T303A by tert-butyl acetylenes: characterization of reactive intermediate adducts to the heme and apoprotein. *Chem Res Toxicol* **15**:1561-1571.

Campbell L, Blackhall F, Thatcher N (2010) Gefitinib for the treatment of non-small-cell lung cancer. *Expert Opin Pharmaco* **11**:1343-1357.

Chen J, Liu D, Zheng X, Zhao Q, Jiang J, Hu P (2015) Relative contributions of the major human CYP450 to the metabolism of icotinib and its implication in prediction of drug-drug interaction between icotinib and CYP3A4 inhibitors/inducers using physiologically based pharmacokinetic modeling. *Expert Opin Drug Met* **11**:857-868.

Ciardiello F, Tortora G (2001) A novel approach in the treatment of cancer: targeting the epidermal growth factor receptor. *Clin Cancer Res* **7**:2958-2970.

FDA (2020) *In Vitro* Metabolism and Transporter Mediated Drug-Drug Interaction Studies Guidance for Industry. Available from: https://www.fda.gov/media/134582/download

Foo W, Tay H, Chan E, Lau A (2015) Meclizine, a pregnane X receptor , is a direct inhibitor and mechanism -based inactivator of human cytochrome P450 3A. *Biochem. Pharmacol*. **97**:320-330.

Hollenberg PF, Kent UM, Bumpus NN (2008) Mechanism-based inactivation of human cytochromes P450s: experimental characterization, reactive intermediates,

and clinical implications. *Chem. Res. Toxicol.* **21**:189-205.

Galetin A, Burt H, Gibbons L, Houston JB (2006) Prediction of time-dependent CYP3A4 drug-drug interactions: impact of enzyme degradation, parallel elimination pathways, and intestinal inhibition [J]. *Drug Metab Dispos* **34**:166-175.

Gridelli C, Maione P, Bareschino MA, Schettino C, Sacco PC, Ambrosio RB, Barbato V, Falanga M, Rossi A (2010) Erlotinib in the treatment of non-small cell lung cancer: current status and future developments. *Anticancer Res* **30**:1301-1310.

Gu A, Shi C, Xiong L, Chu T, Pei J, Han B (2013) Efficacy and safety evaluation of icotinib in patients with advanced non-small cell lung cancer. *Chin J Cancer* **25**:90-94.

Kalgutkar AS, Obach RS, Maurer TS (2007) Mechanism-Based Inactivation of Cytochrome P450 Enzymes: Chemical Mechanisms, Structure-Activity Relationships and Relationship to Clinical Drug-Drug Interactions and Idiosyncratic Adverse Drug Reaction. *Curr Drug Metab* **8**:407447.

Katzenmaier S, Markert C, Riedel KD, Burhenne J, Haefeli WE, Mikus G (2011) Determining the time course of CYP3A inhibition by potent reversible and irreversible CYP3A inhibitors using a limited sampling strategy. *Clin Pharmacol Ther* **90**: 666-673

Keating GM (2014) Afatinib: A review of its use in the treatment of advanced non-small cell lung cancer. *Drugs* **74**:207-221.

Kent UM, Juschyshyn MI, Hollenberg PF (2001) Mechanism-based inactivators as probes of cytochrome P450 structure and function. *Curr Drug Metab* **2**:215-243.

Lim HK, Duczak N Jr, Brougham L, Elliot M, Patel K, and Chan K (2005) Automated screening with confirmation of mechanism-based inactivation of CYP3A4, CYP2C9, CYP2C19, CYP2D6, and CYP1A2 in pooled human liver microsomes.

Drug Metab Dispos **33**:1211-1219.

Lin H, Kent UM, Hollenberg PF (2002) Mechanism-based inactivation of cytochrome P450 3A4 by 17 alpha-ethynylestradiol: evidence for heme destruction and covalent binding to protein. *J Pharmacol Exp Ther* **301**:160-167.

Liu D, Jiang J, Zhang L, Tan F, Wang Y, Hu P (2011) Metabolite characterization of a novel anti-cancer agent, icotinib, in humans through liquid chromatography/quadrupole time-of-flight tandem mass spectrometry. *Rapid Commun Mass Sp* **25**:2131-2140.

Liu D, Zhang L, Wu Y, Jiang J, Tan F, Wang Y, Liu Y, Hu P (2015) Clinical pharmacokinetics, safety, and preliminary efficacy evaluation of icotinib in patients with advanced non-small cell lung cancer. *Lung Cancer* **89**:262-267.

Mao X, Hu Z, Wang Q, Zhang N, Zhou S, Peng Y, and Zheng J (2018) Nitidine Chloride is a mechanism-based inactivator of CYP2D6. *Drug Metab Dispos* **46**: 1137-1145.

McDonald RN, Schwab PA (1964) Strained ring systems. I. peroxidation studies with certain acetylenes. The relevance of oxirene intermediates. *J Am Chem Soc* **86**:4866-4871.

Noriaki Ikemura, Satoshi Yamaori, Chinatsu Kobayashi, Shinobu Kamijo, Norie Murayama, Hiroshi Yamazaki, Shigeru Ohmori (2019) Inhibitory effects of antihypertensive drugs on human cytochrome P450 2J2 activity: Potent inhibition by azelnidipine and manidipine. *Chem-Biol Interact* **306**:1-9.

Obach RS, Walsky RL, Venkatakrishnan K, Houston J B, Tremaine LM (2005) *In vitro* cytochrome P450 inhibition data and the prediction of drug-drug interactions: qualitative relationships, quantitative predictions, and the rank-order approach. *Clin Pharmacol Ther* **78**:582-592.

Orr ST, Ripp SL, Ballard TE, Henderson JL, Scott DO, Obach RS, SUn H, Kalgutkar AS (2012) Mechanism-based inactivation (MBI) of cytochrome P450 enzymes: structure-activity relationships and discovery strategies to mitigate drug-drug interaction risks. *J Med Chem* **55**:4896-4933.

Osawa Y and Pohl LR (1989) Covalent bonding of the prosthetic heme to protein: a potential mechanism for the suicide inactivation or activation of hemoproteins. *Chem Res Toxicol* **2**:131-141.

Ou SHI (2012) Second-generation irreversible epidermal growth factor receptor (EGFR) tyrosine kinase inhibitors (TKIs): a better mousetrap? A review of the clinical evidence. *Crit Rev Oncol Hemat* **83:**407-421.

Pearson RG (1969) Hard and Soft Acids and Bases. *Survey of Progress in Chemistry* **5**:1-52.

Regal KA, Schrag ML, Kent UM, Wienkers LC, Hollenberg PF (2000) Mechanism-based inactivation of cytochrome P450 2B1 by 7-ethynylcoumarin: verification of apo-P450 adduction by electrospray ion trap mass spectrometry. *Chem Res Toxicol* **13**:262-270.

Ruan C, Liu D, Jiang J, Hu P (2012) Effect of the CYP2C19 genotype on the pharmacokinetics of icotinib in healthy male volunteers. *Eur J Clin Pharmacol* **68**:1677-1680.

Shi Y, Zhang L, Liu X, Zhou C, Zhang S, Wang D, Li Q, Qin S, Hu C, Zhang Y, Chen J, Cheng Y, Feng J, Zhang H, Song Y, Wu Y, Xu N, Zhou J, Luo J, Bai C (2013) Icotinib versus gefitinib in previously treated advanced non-small-cell lung cancer (ICOGEN): a randomised, double-blind phase 3 non-inferiority trial. *Lancet Oncol* **14**:953-961.

Silverman RB (1995) Mechanism-based enzyme inactivators. *Method Enzymol*

249:240-283.

Stamos J, Sliwkowski MX, Eigenbrot C (2002) Structure of the epidermal growth factor receptor kinase domain alone and in complex with a 4-anilinoquinazoline inhibitor. *J Biol Chem* **277**:46265-46272.

Tan F, Shen X, Wang D, Xie G, Zhang X, Ding L, Hu Y, He WW, Wang Y (2012) Icotinib (BPI-2009H), a novel EGFR tyrosine kinase inhibitor, displays potent efficacy in preclinical studies. *Lung Cancer* **6**:177-182.

Tan F, Zhang L, Zhao Q, Liu D, Hu Y, Liu Y, Hu Y, Liu Y, Ding L, Hu B, Wang Y (2009) Pharmacology and clinical evaluation of icotinib hydrochloride. *Chinese Journal of New Drugs* **18**:1691-1694.

Vieira MdLT, KirbyB, Ragueneau-Majlessi I, Galetin A, Chien JYL, Einolf JYL, Fahmi OA, Fischer V, Fretland A, Grime K, Hall SD, Higgs R, Plowchalk D, Riley R, Seibert E, Skordos K, Snoeys J, Venkatakrishnan K, Waterhouse T, Obach RS, Berglund EG, Zhang L, Zhao P, Reynolds KS and Huang S (2014) Evaluation of various static *in vitro-in vivo* extrapolation models for risk assessment of the CYP3A inhibition potential of an investigational drug. *Clin Pharmacol Ther* **95**: 189-198.

Wang K, Zheng L, Peng Y, Song J, Zheng J (2014) Selective and sensitive platform for function-based screening of potentially harmful furans. *Anal Chem* **86**:10755-10762.

Wang W, Song Z, Zhang Y (2017) Zoledronic acid as potential efficacy application combined with icotinib for non-small cell lung cancer with bone metastases. *Transl Cancer Res* **6**:129-135.

Wu Q, Liu L, Jiang Y, Shen L, Xu Y (2017) Effect of Chinese medicine treatment based on syndrome differentiation combined with icotinib in treating advanced

non-small cell lung cancer. *Chin J Integr Med* **37**:1054-1058.

Yamreudeewong W, DeBisschop M, Martin LG, Lower DL (2003) Potentially significant drug interactions of class III antiarrhythmic drugs. *Drug Safety* **26**:421-438.

Zhao Q, Wang Y, Tang Y, Peng L (2014) Icotinib combined with rapamycin in a renal transplant recipient with epidermal growth factor receptor-mutated non-small cell lung cancer: A case report. *Oncol Lett* **7**:171-176.

Zhao Y (2017) Feiliu decoction combined with icotinib tablets in the Treatment of Advanced Lung Cancer 30 cases. *Guangming Journal of Chinese Medicine* **32**:2244-2245.

Footnotes. This work was partially supported by the National Natural Science Foundation of China [Grants 81773813 and 81830104] and the Natural Science Foundation of Liaoning Province of China [Grants 201801561].

Conflicts of interest. Authors have no conflict of interest.

DMD Fast Forward. Published on July 26, 2021 as DOI: 10.1124/dmd.121.000369
This article has not been copyedited and formatted. The final version may differ from this version.

Table

Table 1. Protective roles of SOD/catalase and NAL/GSH in CYP3A inhibition induced by ICT.

Figure legends

Figure 1. Chemical structures of compounds employed in the present study.

Figure 2. Time-, concentration-, and NADPH-dependent inhibition of CYP3A by ICT (A). Human hepatic microsomal incubations containing ICT at concentrations of 0 (●), 5 (■), 15 (▲), 25 (×), 35 (◆) and 50 μM (○) supplemented with NADPH were conducted for 0, 10, 20 and 30 min at 37 °C and then submitted to CYP3A activity measurement. B: Wilson's plot. The estimation of K_{obs} was achieved by calculation of the slope of the regression lines as A indicates. C: NADPH-dependent inhibition of CYP3A by ICT. Human liver microsomes mixed with ICT at concentrations of 0 (●) or 50 μM without (■) or with (○) NADPH was incubated at 37 °C for various time periods and then submitted to CYP3A activity measurement. Data represent the mean ± SD (n = 3).

Figure 3. Protection of CYP3A by nifedipine from ICT-induced inactivation. NADPH-fortified human liver microsomes were incubated with ICT (50 μM) + nifedipine (○, 100 μM), ICT alone (■), nifedipine alone (▼), or vehicle (●) for 0, 10, 20 and 30 min at 37 °C and then submitted to CYP3A activity measurement. Data represent the mean ± SD (n = 3).

Figure 4. Loss of CYP3A4 (A) and 3A5 (B) activity as a function of the [ICT]/[CYP3A4] or [ICT]/[CYP3A5] molar ratio. The incubation mixture contained

recombinant CYP3A4 or CYP3A5 and ICT at concentrations of 0, 3.125, 6.25, 12.5, 25, 50, 75, 100, or 200 μM. Data represent mean ± SD (n = 3). $P + 1$ value was estimated by extrapolation from the point of intersection to the abscissa.

Figure 5. Biomimetic chemical synthesis of adduct **5** and proposed bioactivation pathway for the formation of adduct **5**.

Figure 6. Identification of ICT-BBA adduct. Ion chromatograms of *m/z* 593→479 obtained from analysis of human liver microsomes without (A) and with (C) NADPH. Ion chromatograms of *m/z* 595→481 obtained from analysis of human liver microsomes without (B) and with (D) NADPH. MS/MS spectra obtained from enhanced product ion scanning of ICT-BBA adduct of *m/z* 593 (E) and 595 (F).

Figure 7. Characterization of synthetic ICT-BBA adduct **5**. Ion chromatograms of *m/z* 595→481 obtained from analysis of microsomal reactions (A) and biomimetic chemical synthesis (B). MS/MS spectra obtained from enhanced product ion scanning of compound **5** detected in microsomal incubations (C) and biomimetic chemical synthesis (D).

Figure 8. Time-dependent inhibition of CYP3A by ICT and its analogs. NADPH-supplemented human liver microsomes were individually incubated with vehicle (●), ICT (■), **2** (▲), or **3** (×**)** for 0, 10, 20 and 30 min at 37 °C and then submitted to CYP3A activity measurement. The resulting enzyme activities examined were calculated by determination of peak area ratio of the analytes vs internal standard. Normalization was established by determination of the enzymatic activity ratio at 0 min vs that of each time points. Data represent the mean ± SD (n = 3).

Figure 9. Recombinant human P450s responsible for the generation of the ketene intermediate. ICT was individually incubated with recombinant human P450s supplemented with NADPH and BBA, followed by submitting to LC-MS/MS analysis. The production of ICT-BBA adduct in incubation mixtures of ICT exposed with CYP3A4 was defined as 100% in comparison with that incubated with other recombinant human P450s. Data represent mean ± SD (n = 3).

Figure 10. Representative MRM chromatograms for propranolol (A, C, and E, *m/z* 260→116) and heme (B, D, and F, *m/z* 616→557) acquired from analyses of propranolol (A), authentic hemin standard (B), and incubation mixtures fortified with ICT and CYP3A4 without (C and D) or with (E and F) NADPH.

Figure 11. MS/MS spectrum of hemin.

DMD Fast Forward. Published on July 26, 2021 as DOI: 10.1124/dmd.121.000369
This article has not been copyedited and formatted. The final version may differ from this version.

	Remaining activity (%)
ICT	38.1 ± 4.4
ICT + SOD/Catalase	32.4 ± 2.2
ICT + GSH/NAL	40.5 ± 6.3

Table 1

DMD Fast Forward. Published on July 26, 2021 as DOI: 10.1124/dmd.121.000369
This article has not been copyedited and formatted. The final version may differ from this version.

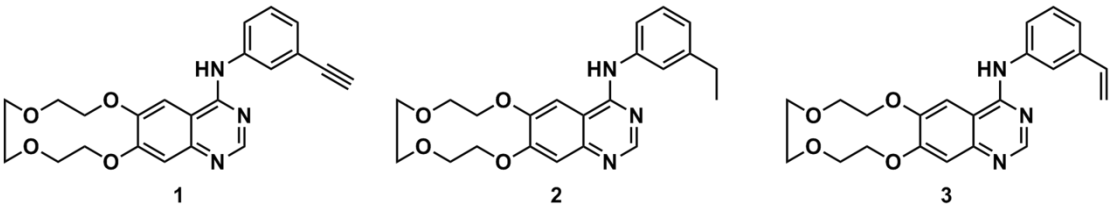

Figure 1

DMD Fast Forward. Published on July 26, 2021 as DOI: 10.1124/dmd.121.000369
This article has not been copyedited and formatted. The final version may differ from this version.

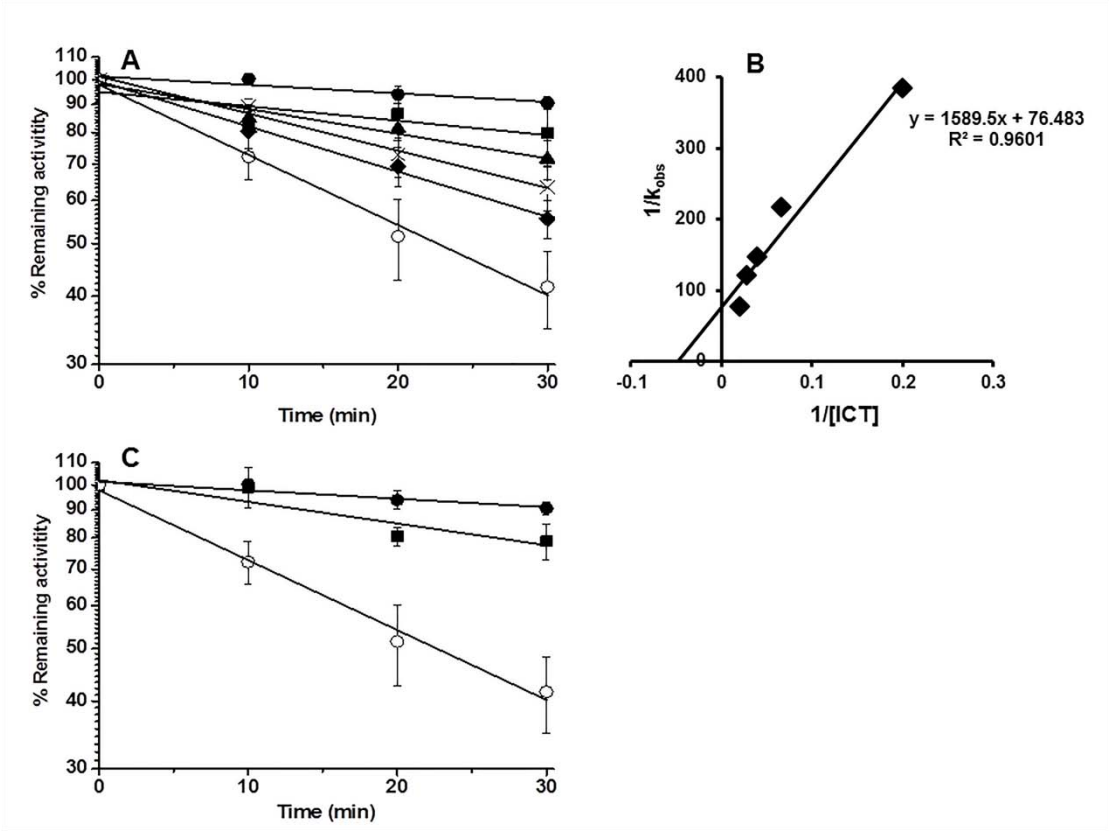

Figure 2

DMD Fast Forward. Published on July 26, 2021 as DOI: 10.1124/dmd.121.000369
This article has not been copyedited and formatted. The final version may differ from this version.

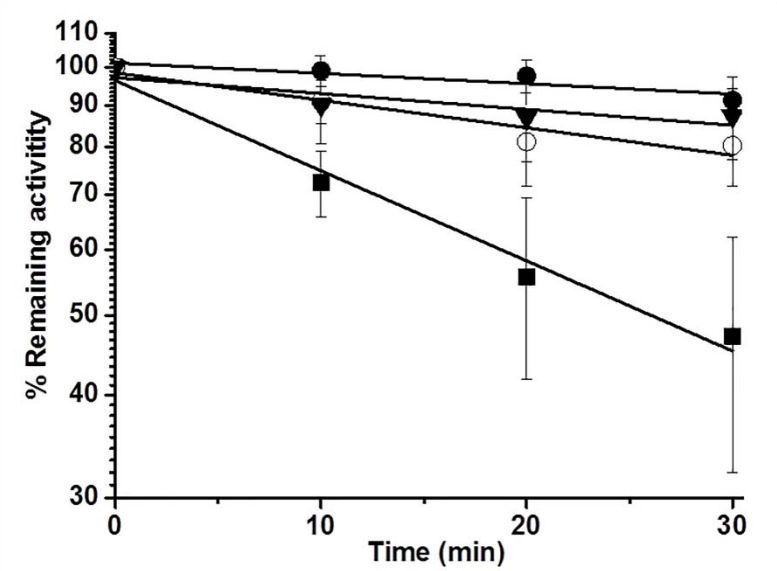

Figure 3

DMD Fast Forward. Published on July 26, 2021 as DOI: 10.1124/dmd.121.000369
This article has not been copyedited and formatted. The final version may differ from this version.

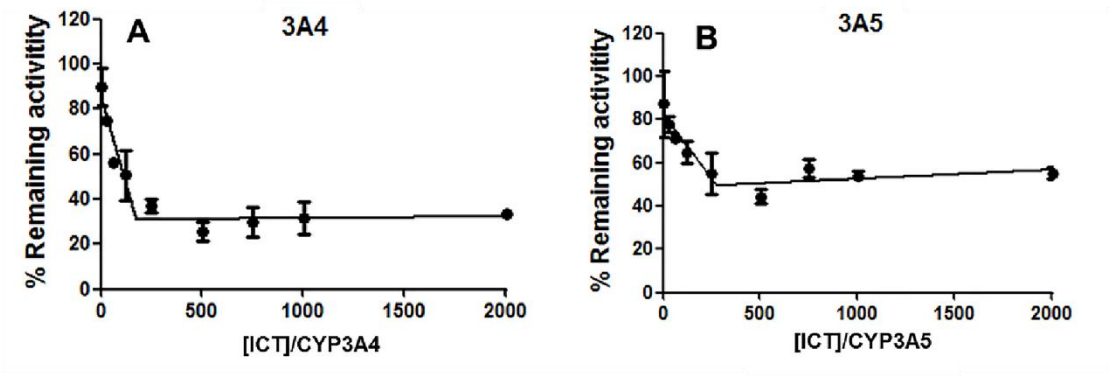

Figure 4

DMD Fast Forward. Published on July 26, 2021 as DOI: 10.1124/dmd.121.000369
This article has not been copyedited and formatted. The final version may differ from this version.

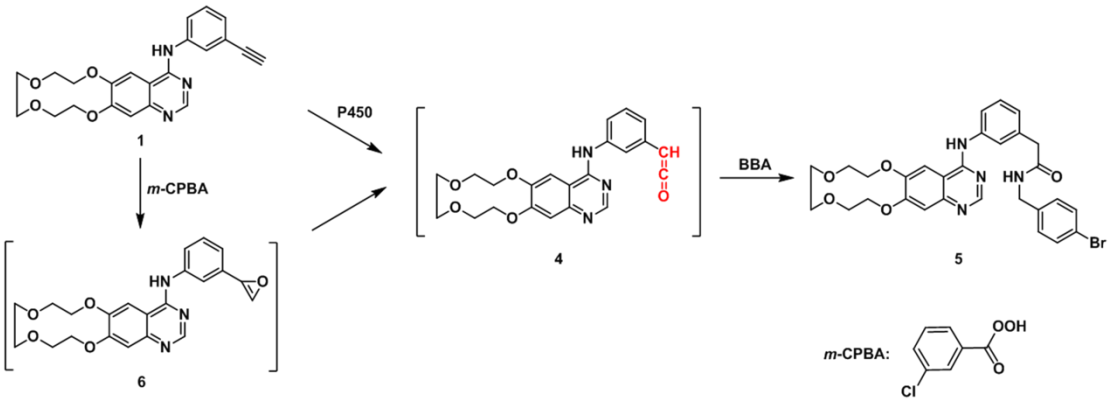

Figure 5

DMD Fast Forward. Published on July 26, 2021 as DOI: 10.1124/dmd.121.000369
This article has not been copyedited and formatted. The final version may differ from this version.

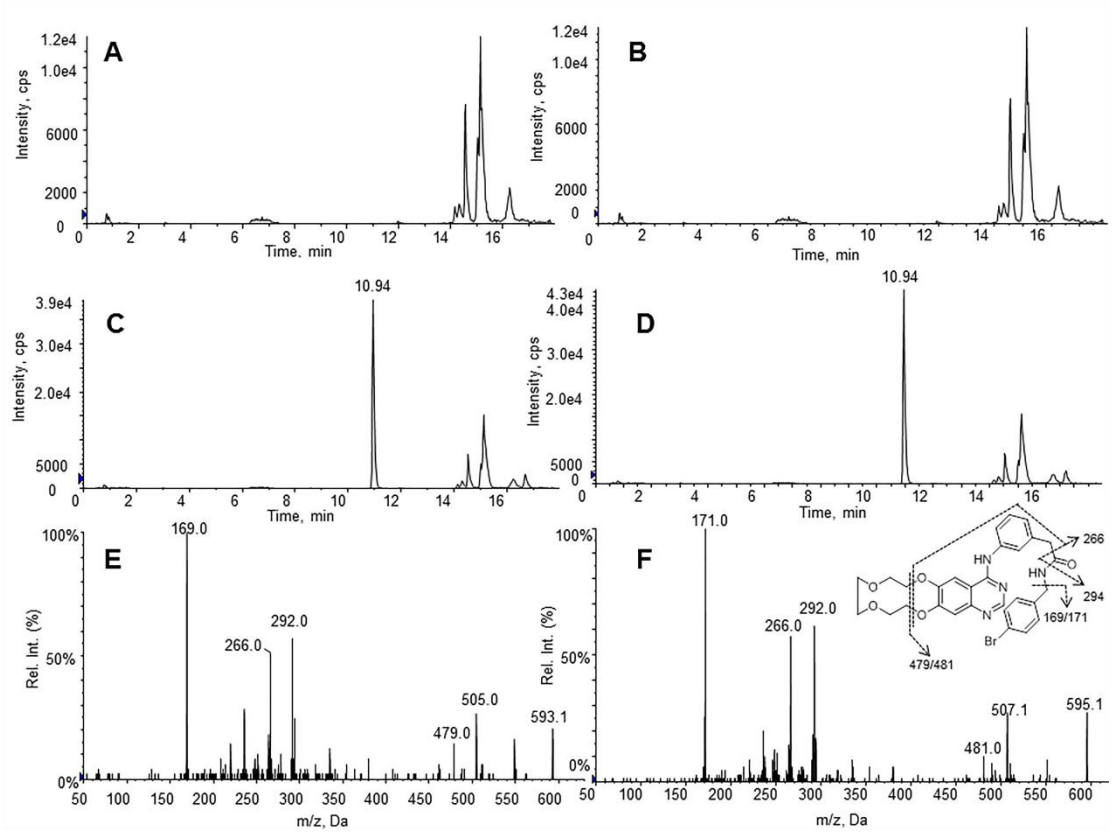

Figure 6

DMD Fast Forward. Published on July 26, 2021 as DOI: 10.1124/dmd.121.000369
This article has not been copyedited and formatted. The final version may differ from this version.

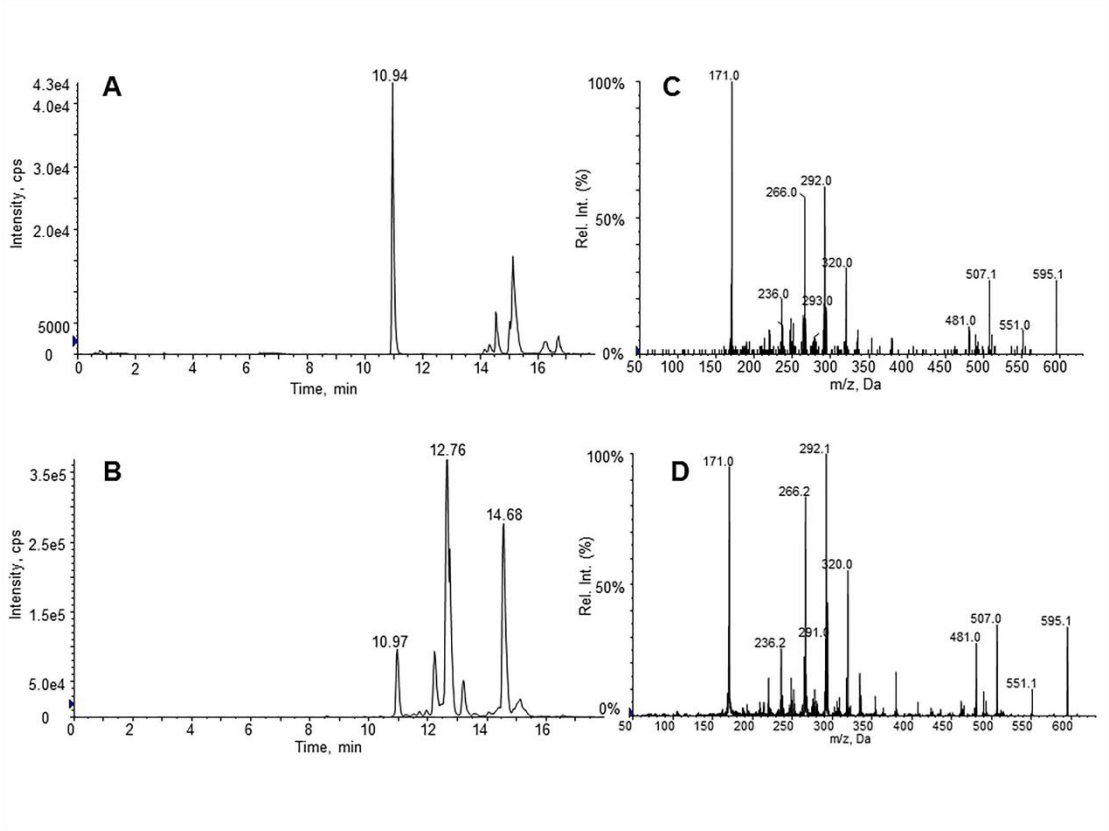

Figure 7

DMD Fast Forward. Published on July 26, 2021 as DOI: 10.1124/dmd.121.000369
This article has not been copyedited and formatted. The final version may differ from this version.

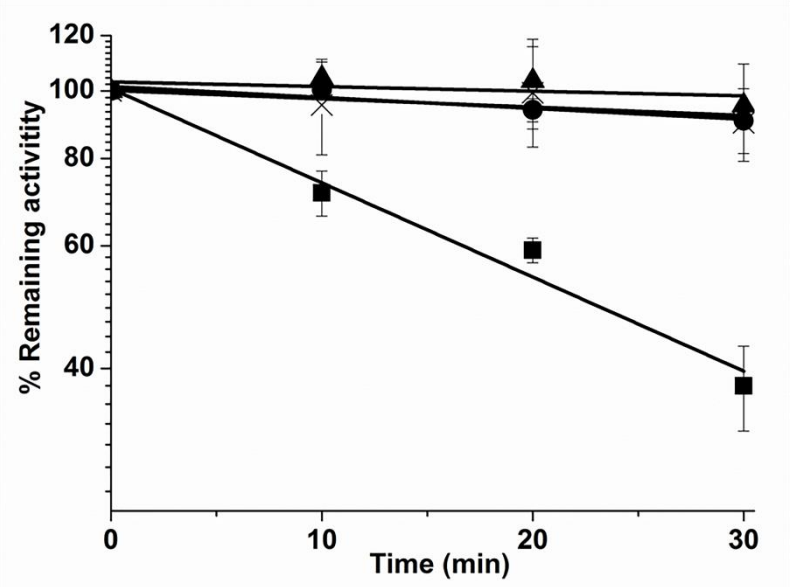

Figure 8

DMD Fast Forward. Published on July 26, 2021 as DOI: 10.1124/dmd.121.000369
This article has not been copyedited and formatted. The final version may differ from this version.

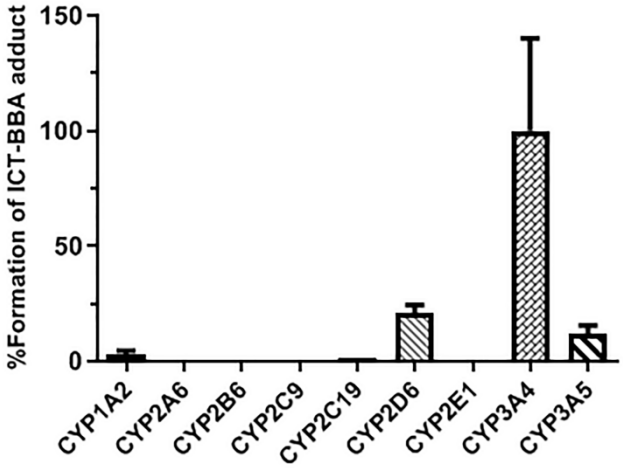

Figure 9

DMD Fast Forward. Published on July 26, 2021 as DOI: 10.1124/dmd.121.000369
This article has not been copyedited and formatted. The final version may differ from this version.

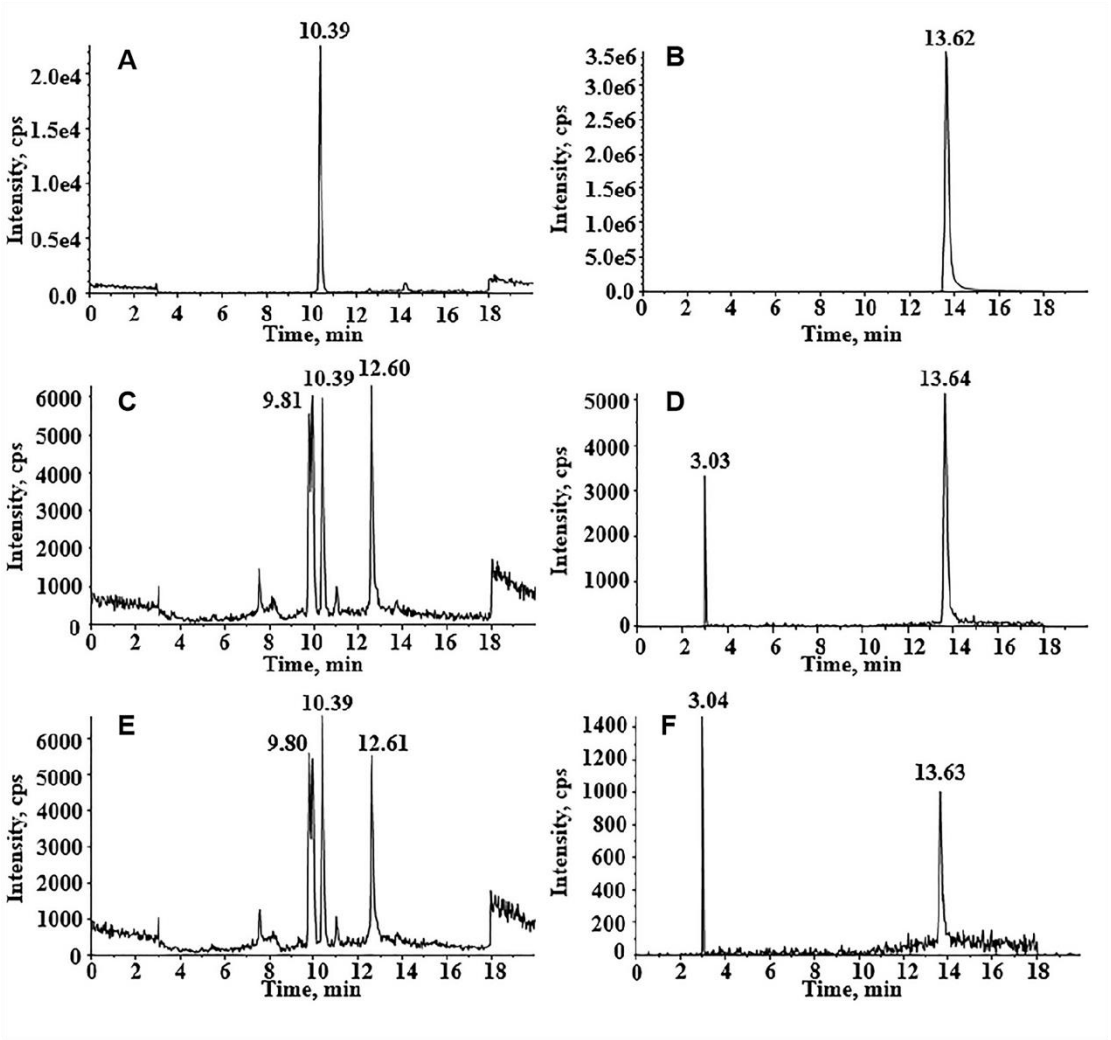

Figure 10

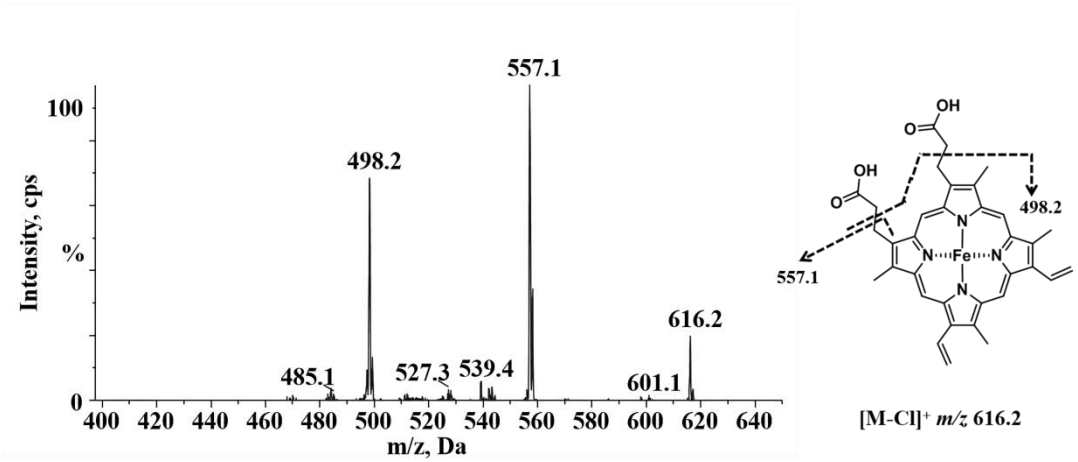

Figure 11

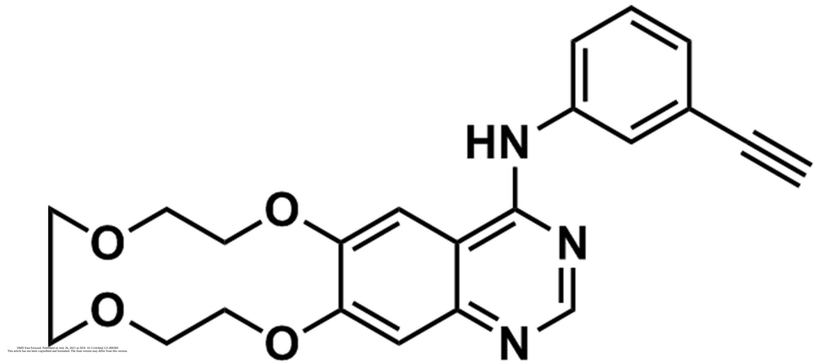

1

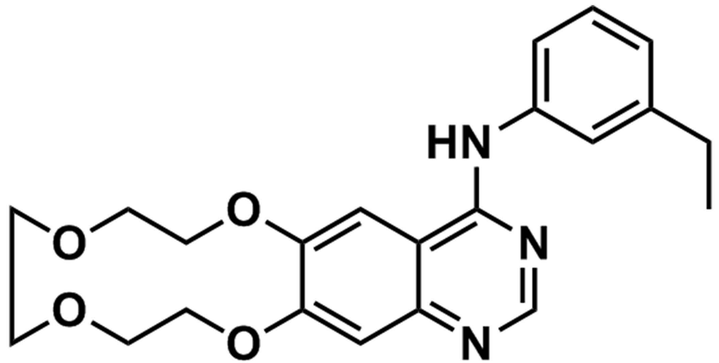

2

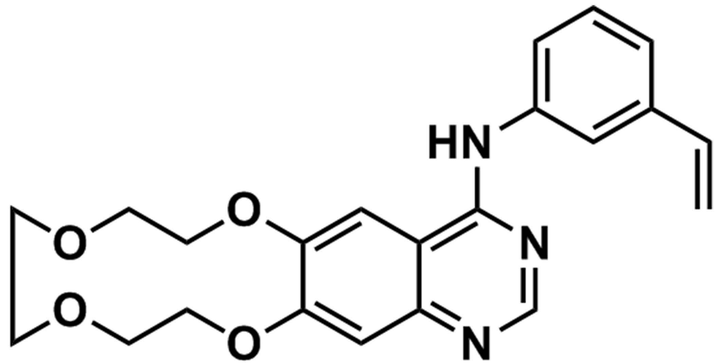

3

Figure 1

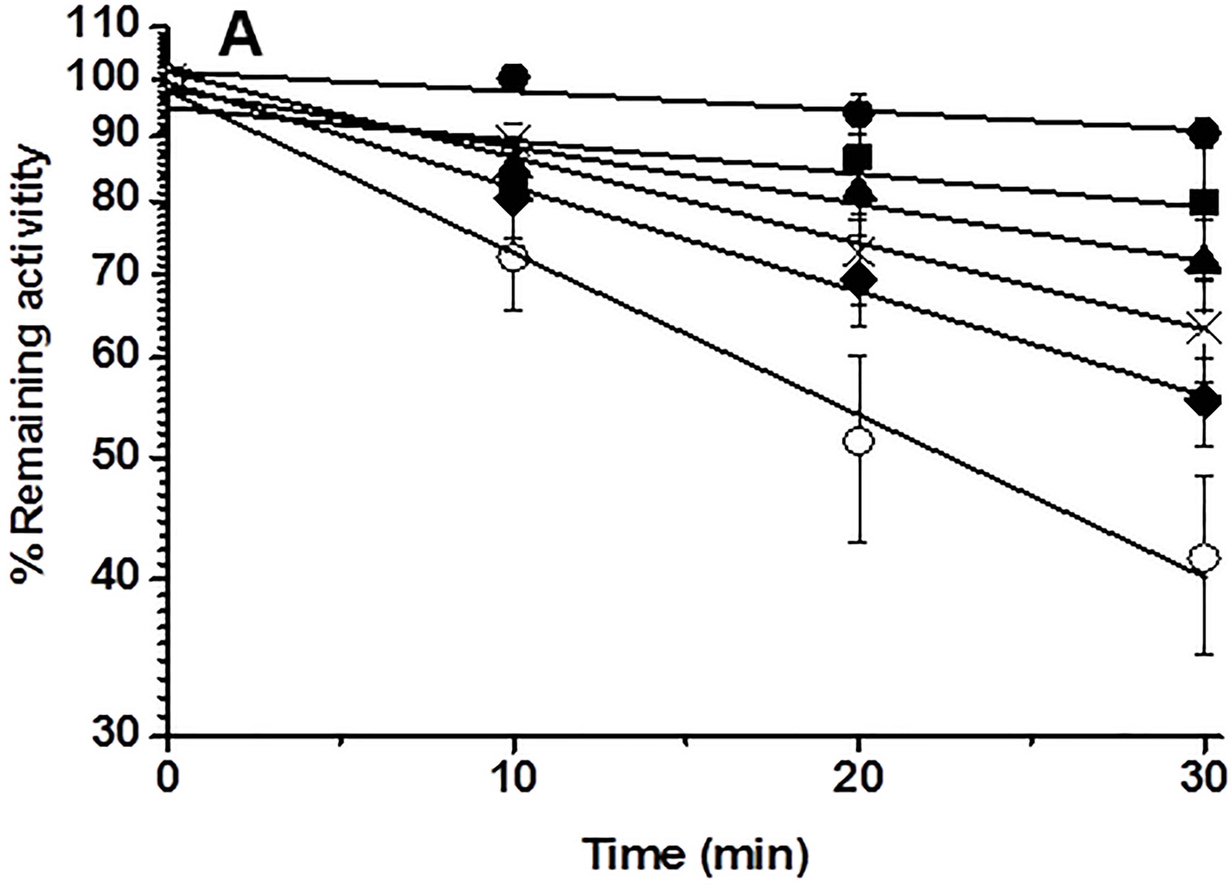
A
% Remaining activitity
Time (min)
110
100
90
80
70
60
50
40
30
0
10
20
30

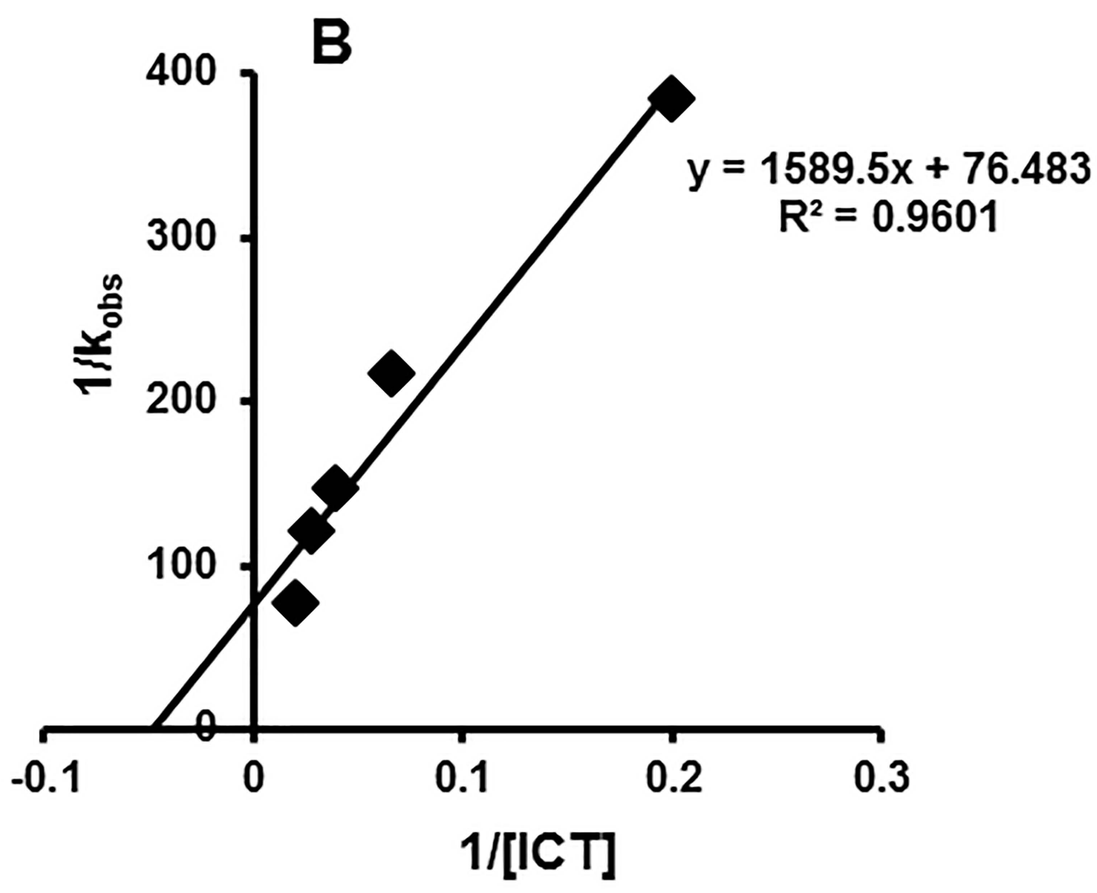
B
y = 1589.5x + 76.483
R² = 0.9601
1/k_obs
1/[ICT]
400
300
200
100
0
-0.1
0
0.1
0.2
0.3

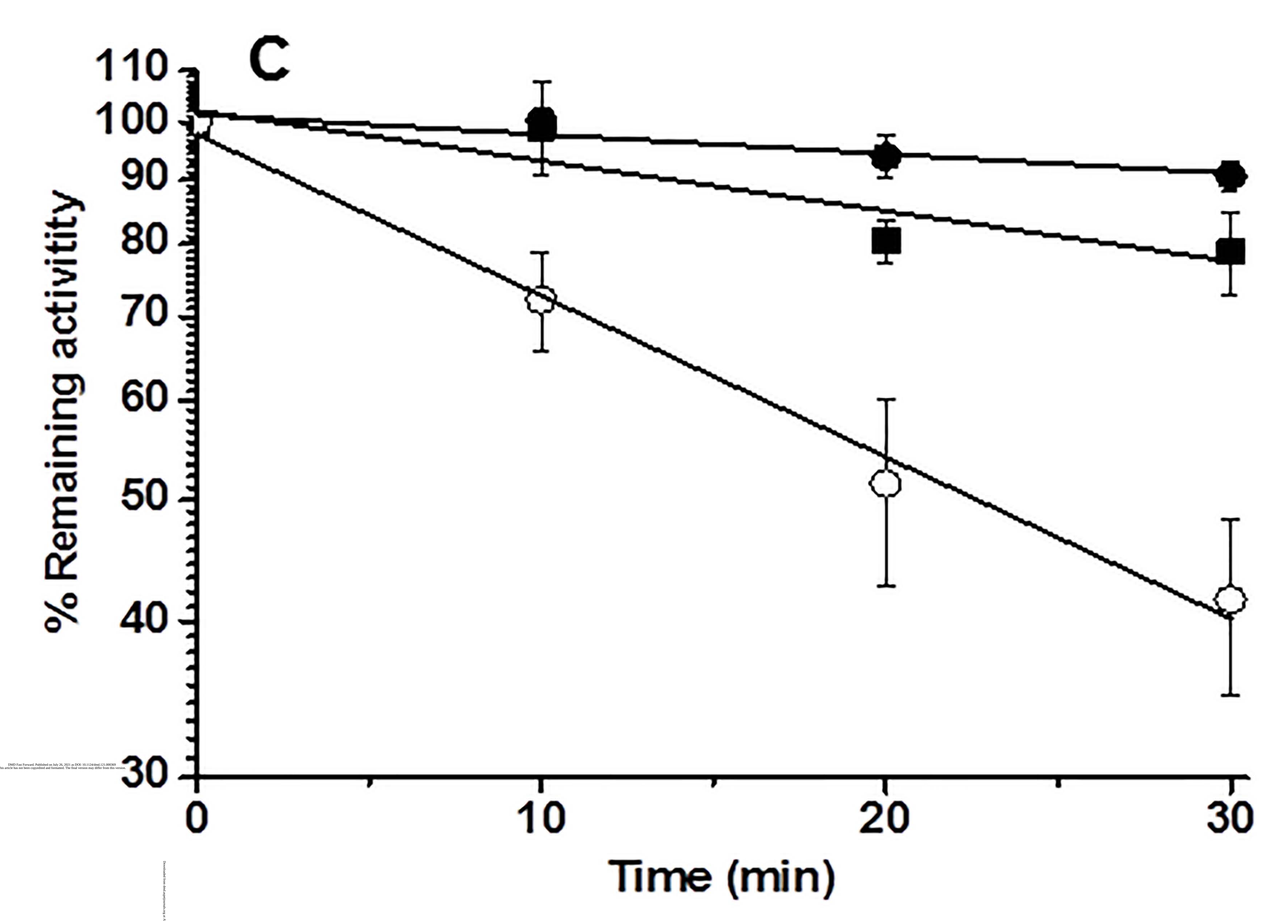
C
% Remaining activitity
Time (min)
110
100
90
80
70
60
50
40
30
0
10
20
30

Figure 2

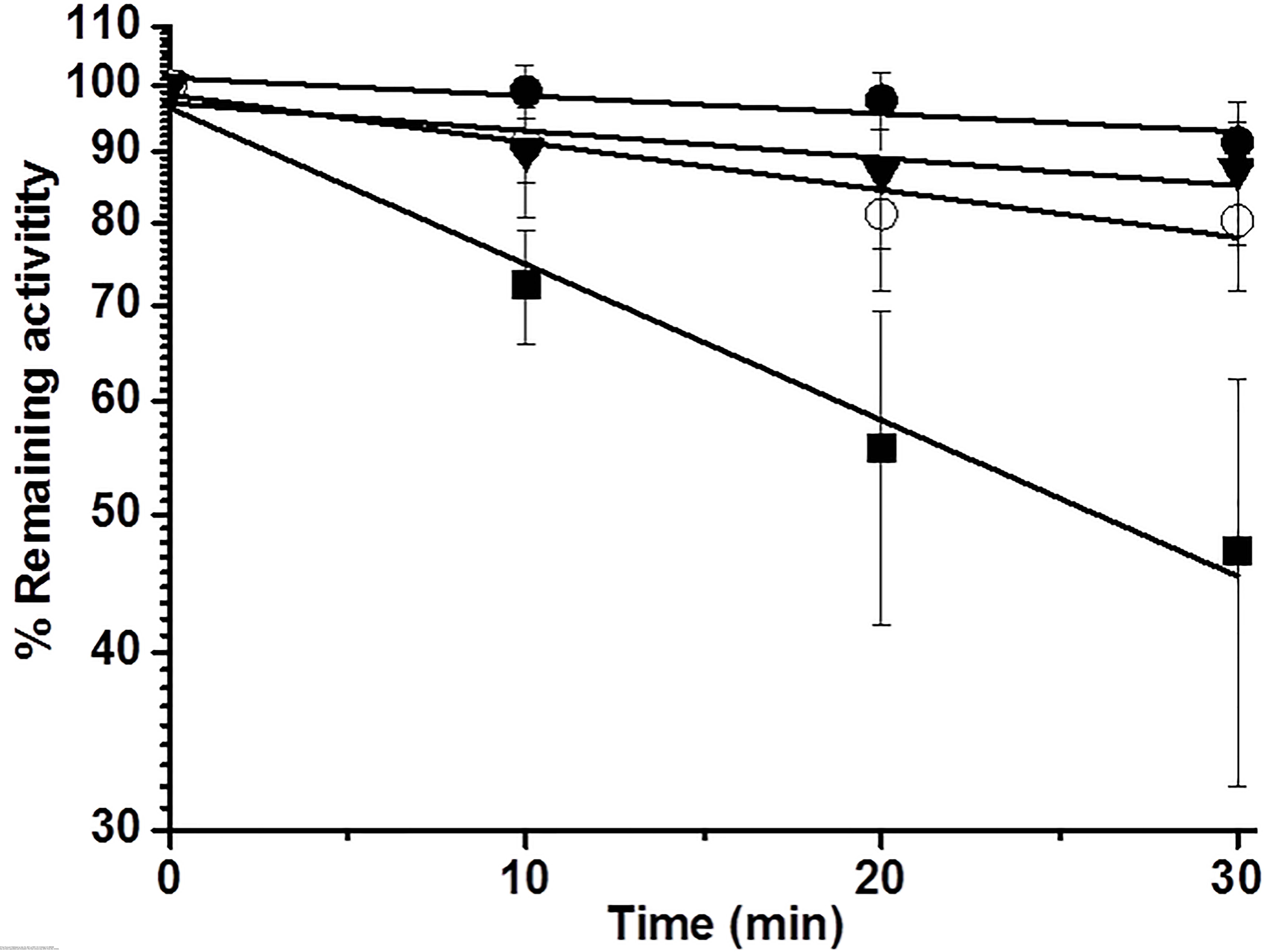
110
100
90
80
70
60
50
40
30
% Remaining activitity
0
10
20
30
Time (min)

Figure 3

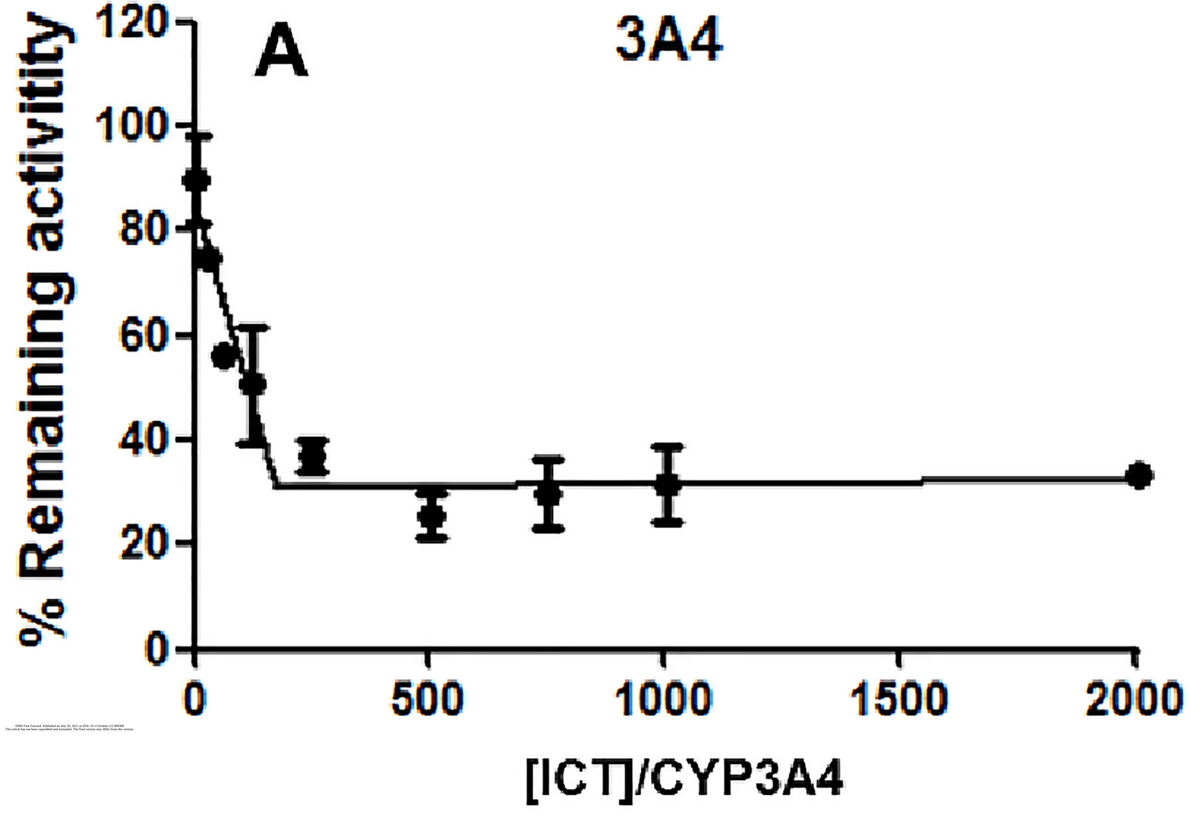
A
3A4
% Remaining activitity
120
100
80
60
40
20
0
0
500
1000
1500
2000
[ICT]/CYP3A4

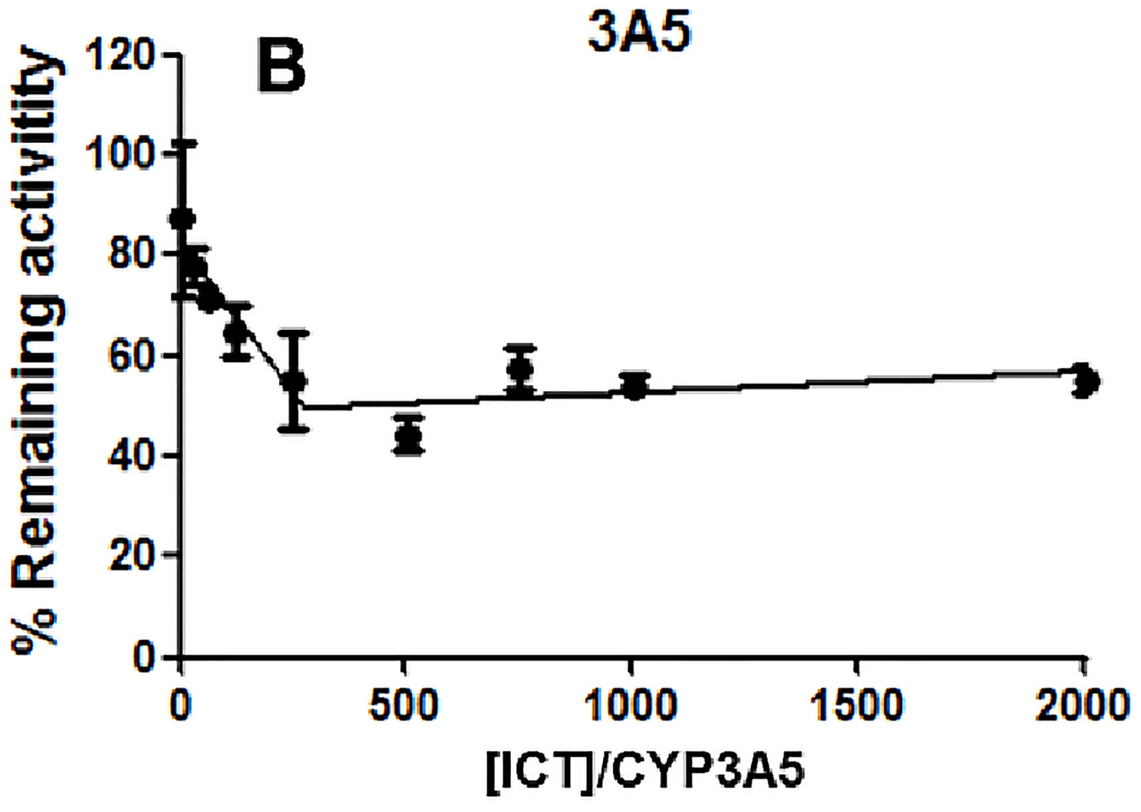
B
3A5
% Remaining activitity
120
100
80
60
40
20
0
0
500
1000
1500
2000
[ICT]/CYP3A5

Figure 4

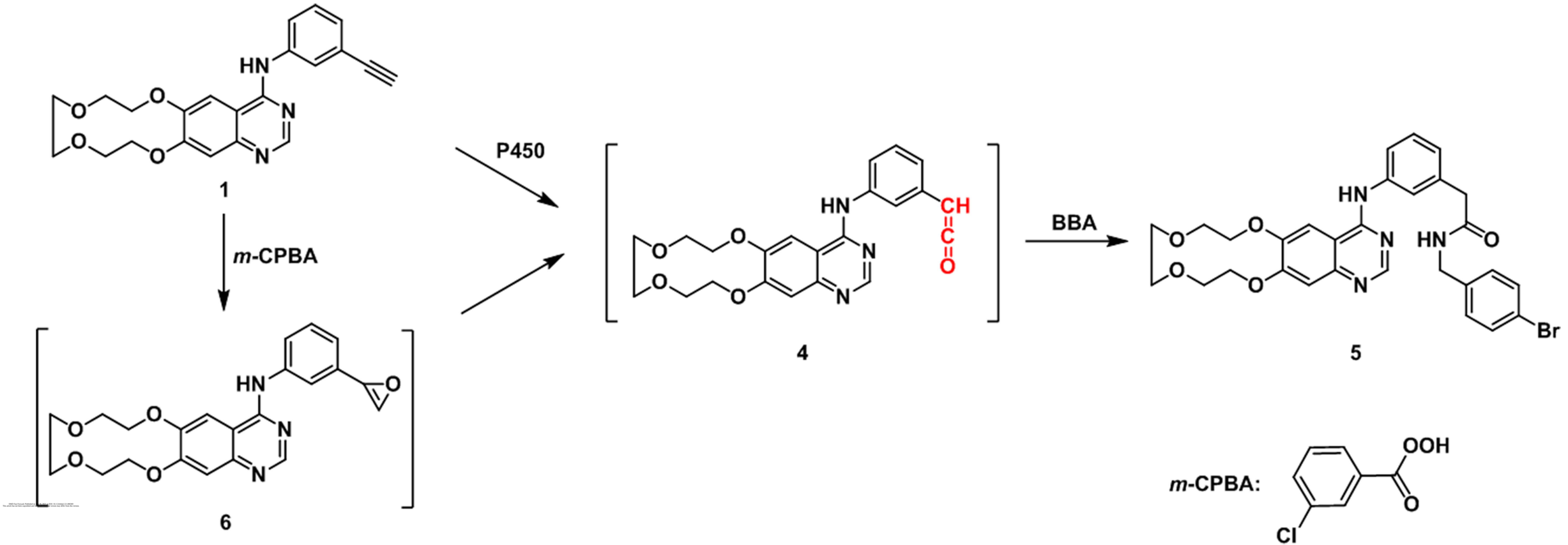

Figure 5

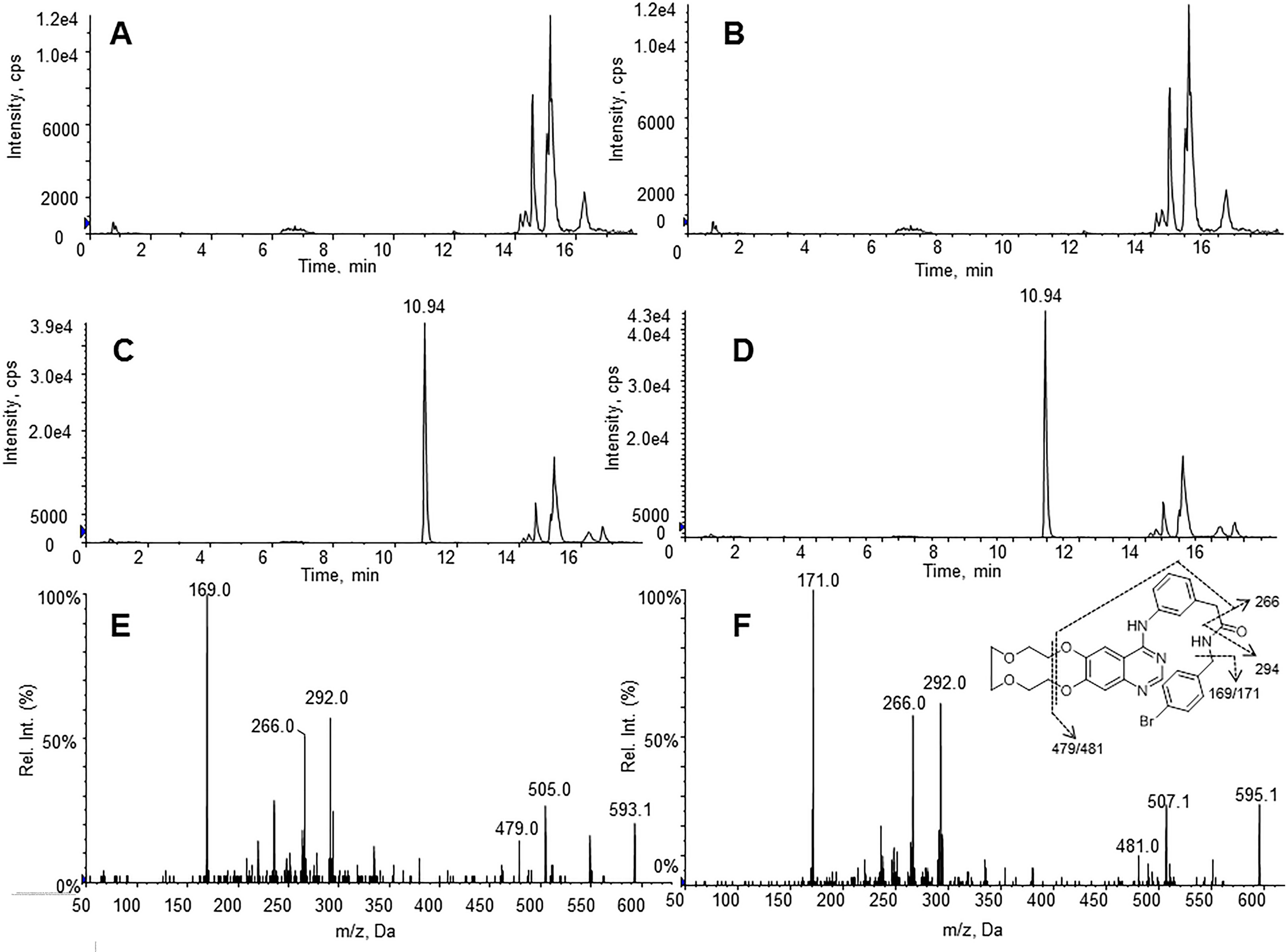
A
B
C
D
E
F
Intensity, cps
Time, min
10.94
169.0
292.0
266.0
505.0
479.0
593.1
171.0
507.1
595.1
481.0
Rel. Int. (%)
m/z, Da
HN
O
N
Br
266
294
169/171
479/481

Figure 6

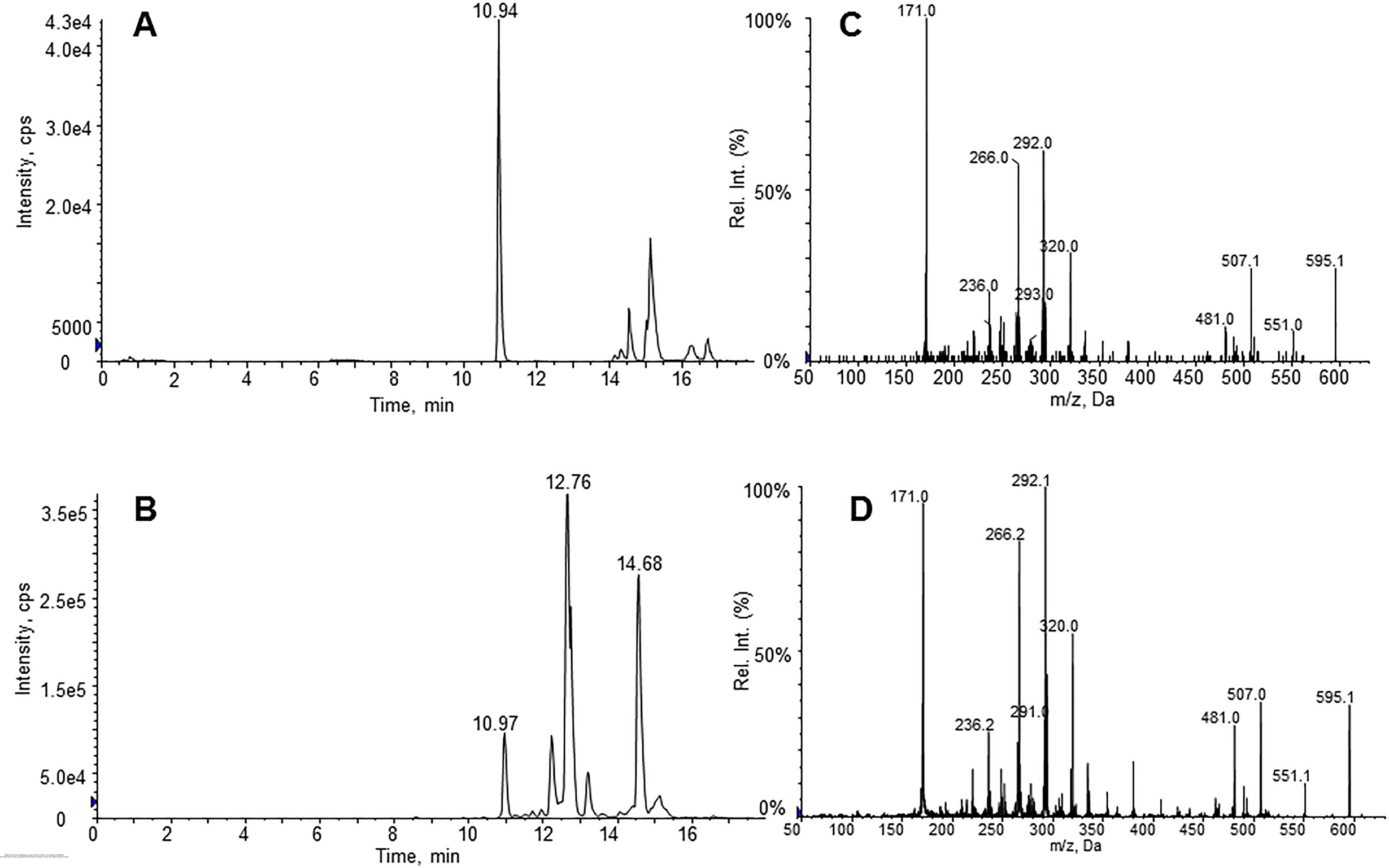
A
10.94
Intensity, cps
Time, min
B
12.76
14.68
10.97
C
171.0
292.0
266.0
320.0
507.1
595.1
236.0
293.0
481.0
551.0
Rel. Int. (%)
m/z, Da
D
171.0
292.1
266.2
320.0
507.0
595.1
291.0
236.2
481.0
551.1

Figure 7

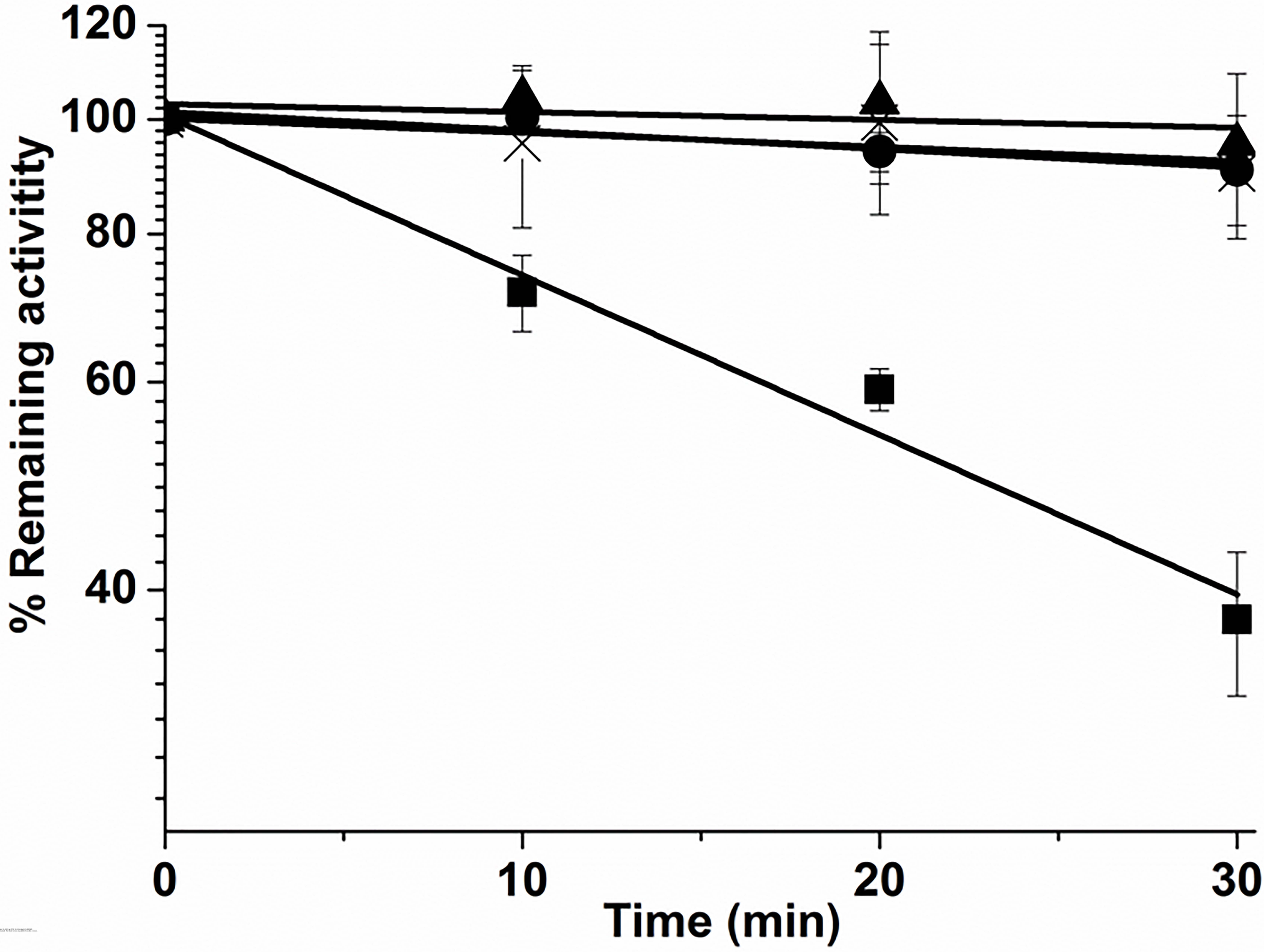

Figure 8

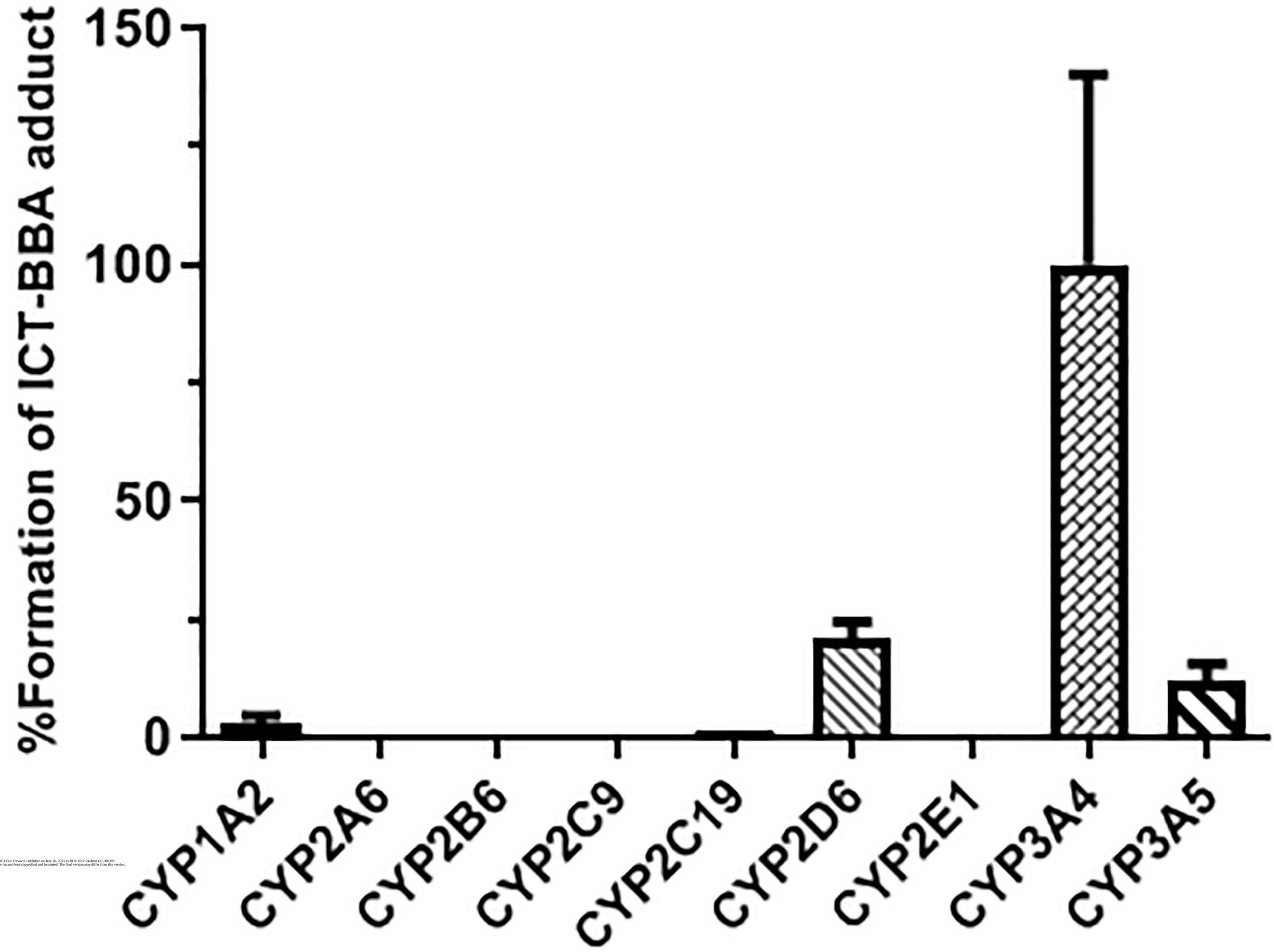

Figure 9

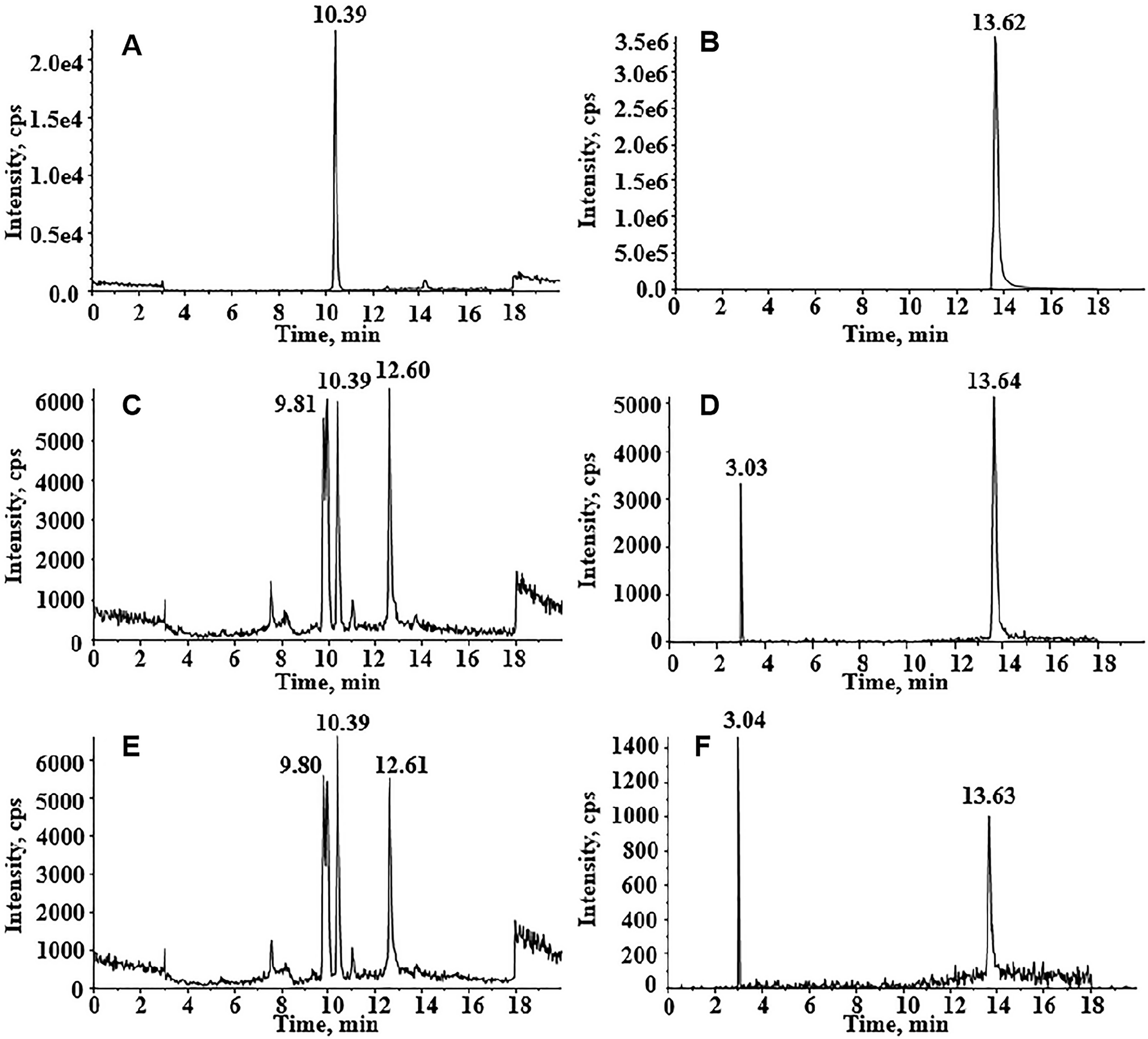
A
10.39
Intensity, cps
Time, min
B
13.62
Intensity, cps
Time, min
C
9.81
10.39
12.60
Intensity, cps
Time, min
D
3.03
13.64
Intensity, cps
Time, min
E
9.80
10.39
12.61
Intensity, cps
Time, min
F
3.04
13.63
Intensity, cps
Time, min

Figure 10

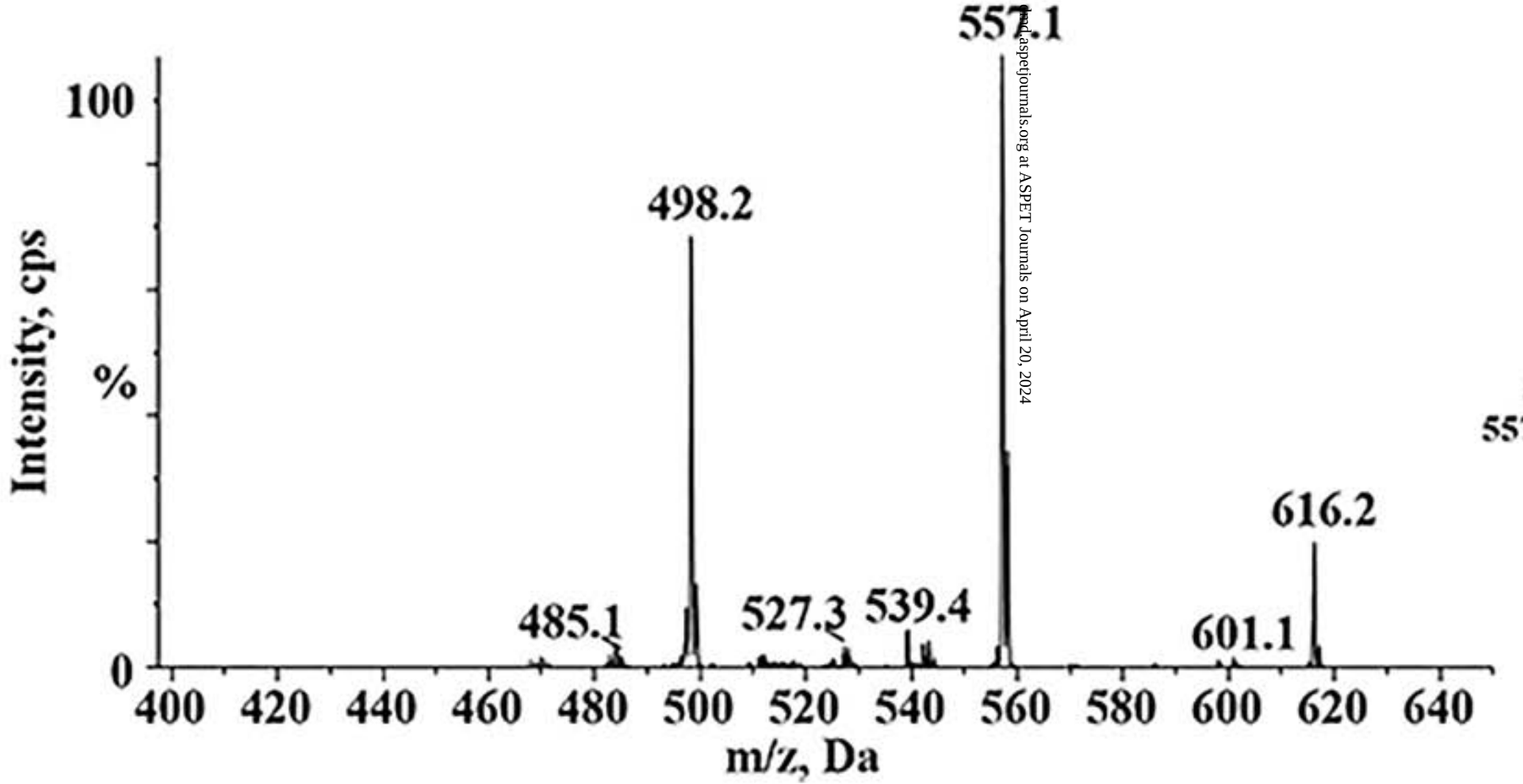

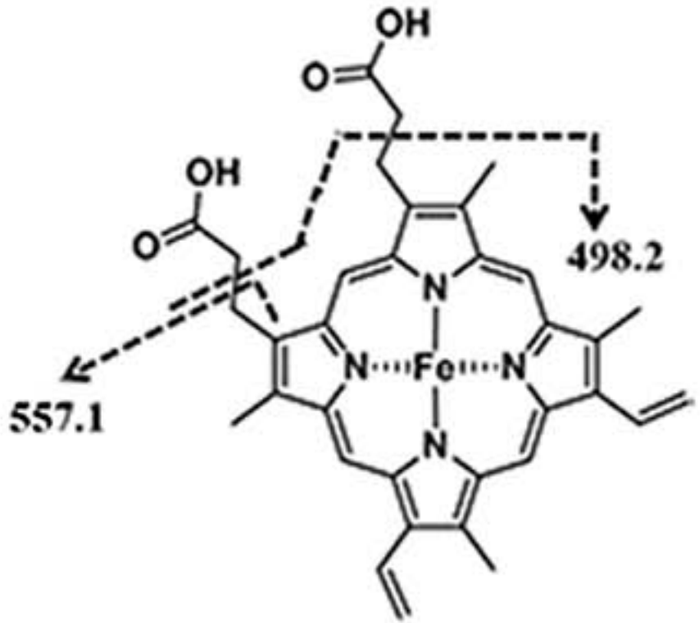

[M-Cl]$^+$ *m/z* 616.2

Figure 11

Supplemental Data for *Drug Metabolism and Disposition*

Icotinib induces mechanism-based inactivation of rhCYP3A4/5 possibly via heme destruction by ketene intermediate

Chen Sun [#], Huimin Zhao[#], Wei Li, Yudi Jia, Yi Yang, Ying Peng, and Jiang Zheng

Wuya College of Innovation (C.S., H.Z., W.L., Y.J., Y.Y., Y.P., J.Z.), School of Pharmaceutical Engineering, Shenyang Pharmaceutical University, Shenyang, Liaoning, 110016, P.R. China; State Key Laboratory of Functions and Applications of Medicinal Plants, Guizhou Provincial Key Laboratory of Pharmaceutics (J.Z.), Guizhou Medical University, Guiyang, Guizhou, 550004, P. R. China; [¶]Key Laboratory of Environmental Pollution Monitoring and Disease Control (J.Z.), Ministry of Education, Guizhou Medical University, Guiyang, 550025, P. R. China.

[#]Authors contributed equally to this work.

[*]**Correspondence authors:**
Jiang Zheng, Ph.D.
Wuya College of Innovation, Shenyang Pharmaceutical University, Shenyang, Liaoning, 110016, P. R. China;
State Key Laboratory of Functions and Applications of Medicinal Plants, Guizhou Provincial Key Laboratory of Pharmaceutics, Guizhou Medical University, Guiyang, Guizhou, 550004, P. R. China.
Email: zhengneu@yahoo.com
Tel: +86-24-23986361
Fax: +86-24-23986510

The two corresponding units contributed equally to this work.

Ying Peng, Ph.D.
Wuya College of Innovation, Shenyang Pharmaceutical University, PO Box 21,103 Wenhua Road, Shenyang 110016, P. R. China
Email: yingpeng1999@163.com
Tel: +86-24-23986361
Fax: +86-24-23986510

Contents

Supplemental Figure 6. Screening of time-dependent inhibition of CYP3A by ICT. NADPH-fortified human hepatic microsomes mixed with ICT at 0 (●) and 50 μM (▲) were incubated at 37 °C for various time periods and then submitted to enzyme activity measurement. Normalization was achieved by determination of enzymatic activity ratio at 0 min vs that of each time points. Data represent the mean ± SD (n = 3). * indicates the significance of the remaining enzyme activity of experimental groups in respect of that of control at the same time point (30 min) of incubations. Levels are considered significant at $^{**}p<0.01$.

Supplemental Figure 7. Equations to calculate the R_2 value for basic models of time-dependent inhibition (FDA, 2020)

Donor Number	Gender	Age	Race	Cause of Death	Smoker	Serology testing
HM-03-006	Male	26	Mongolian	Trauma	Non smoker	Negative
HM-03-007	Male	24	Mongolian	Trauma	Non smoker	Negative
HM-03-008	Male	28	Mongolian	Trauma	Smoker	Negative
HM-03-011	Male	24	Mongolian	Trauma	Smoker	Negative
HM-03-012	Male	29	Mongolian	Trauma	Smoker	Negative
HM-03-013	Male	38	Mongolian	Trauma	Smoker	Negative
HM-03-014	Male	25	Mongolian	Trauma	Smoker	Negative
HM-03-015	Male	28	Mongolian	Trauma	Smoker	Negative
HM-02-001	Male	31	Mongolian	Trauma	Smoker	Negative
HM-02-002	Male	21	Mongolian	Trauma	Non smoker	Negative
HM-06-002	Male	35	Mongolian	Trauma	Smoker	Negative

Supplemental Table 1. Donor information about mixed male human liver microsomes

Time (min)	Flow rate (mL/min)	Solvents	
		CH_3CN in 0.1% HCO_2H (%)	H_2O with 0.1% HCO_2H (%)
0	1.0	30	70
2.0	1.0	30	70
10	1.0	75	25
10.1	1.0	90	10
11	1.0	90	10
11.1	1.0	30	70
13	1.0	30	70

Supplemental Table 2. Gradient elution protocol for separation of 6β-hydroxytestosterone.

Time (min)	Flow rate (mL/min)	Solvents	
		CH_3CN in 0.1% HCO_2H (%)	H_2O with 0.1% HCO_2H (%)
0	0.8	10	90
2.0	0.8	10	90
12	0.8	60	40
12.1	0.8	95	5
16	0.8	95	5
16.1	0.8	10	90
18	0.8	10	90

Supplemental Table 3. Gradient elution protocol for separation of possible ICT-BBA adducts.

Time (min)	Flow rate (mL/min)	Solvents	
		CH_3OH (%)	H_2O with 0.1% HCO_2H (%)
0	0.8	30	70
2.0	0.8	30	70
10	0.8	80	20
15	0.8	80	20
15.5	0.8	95	5
16.5	0.8	95	5
17	0.8	30	70
20	0.8	30	70

Supplemental Table 4. Gradient elution protocol for separation of heme and propranolol.

Time (min)	Flow rate (nL/min)	Solvents	
		CH_3CN in 0.1% HCO_2H (%)	H_2O with 0.1% HCO_2H (%)
0	600	6	94
5.0	600	9	91
20	600	14	86
50	600	30	70
58	600	40	60
60	600	95	5

Supplemental Table 5. Gradient elution protocol for separation of peptides.

Concentration (ng/mL)	Intra-day RSD (%, n = 6)	Inter-day RSD (%, n = 6)	Matrix effect (%, mean ± SD, n = 6)	Stability (n = 3)			
				25 °C in 12 h		4 °C in 48 h	
				RE (%)	RSD (%)	RE (%)	RSD (%)
10.00	7.2 12.7 3.7	9.4	-	-	-	-	-
12.50	4.3 12.5 8.6	8.9	103.6 ± 9.0	-9.6	5.3	12.3	2.3
75.00	1.6 5.0 4.9	4.4	97.6 ± 8.1	-11.4	2.1	-0.6	4.4
175.00	9.0 1.1 7.2	9.1	98.2 ± 4.4	4.2	4.0	1.5	2.5

Supplemental Table 6. Precision, accuracy, matrix effect and stability of 6β-hydroxytestosterone in LLOQ (10 ng/mL) and QC samples

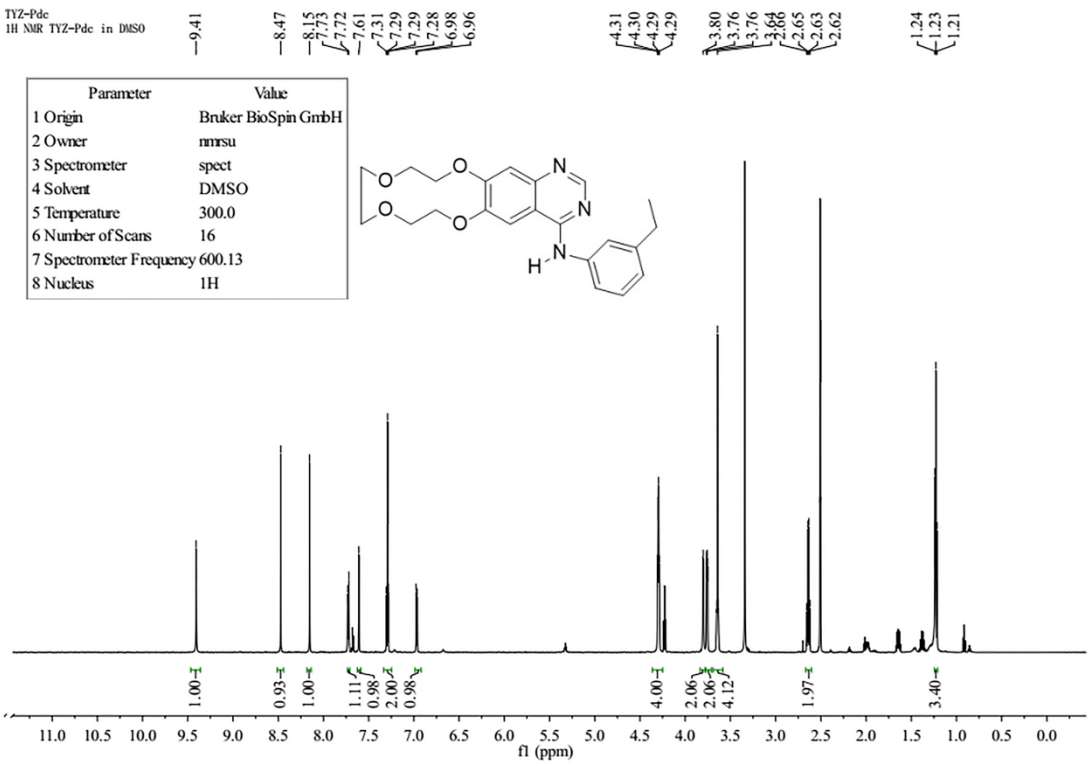

Supplemental Figure 1. ^{1}H NMR spectrum of ethyl analog of ICT.

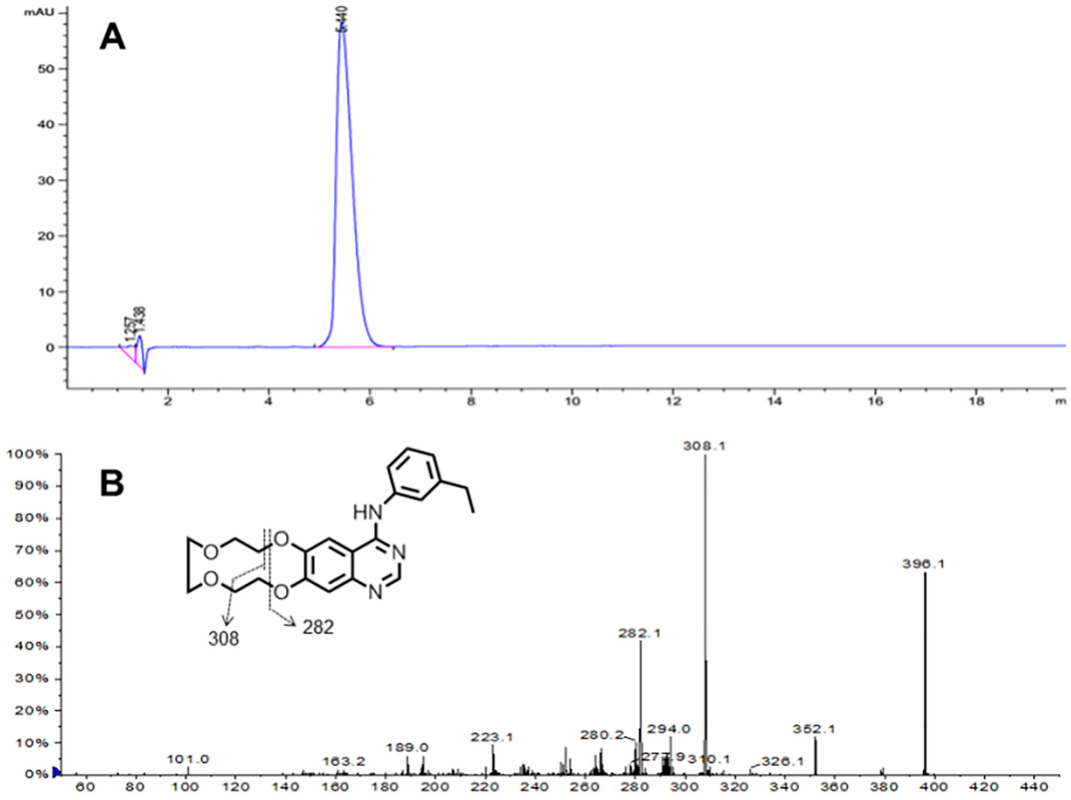

Supplemental Figure 2. HPLC-UV (A) and MS/MS (B) spectra of ethyl analog of ICT

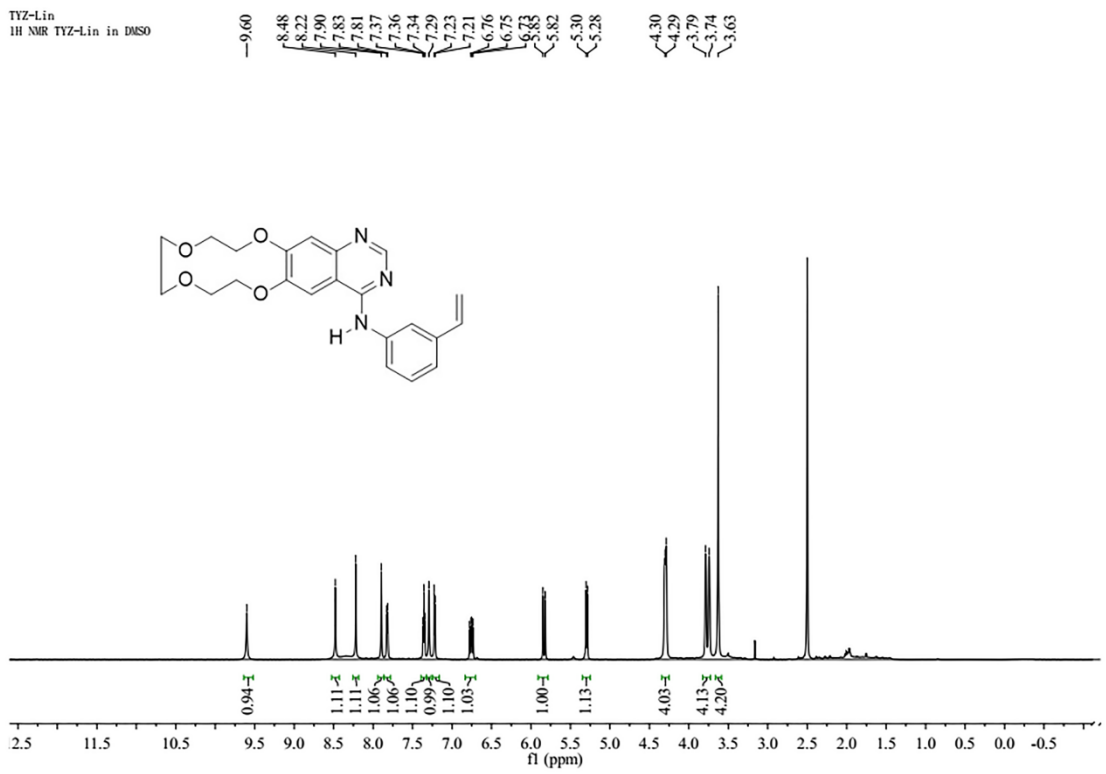

Supplemental Figure 3. ^{1}H NMR spectrum of vinyl analog of ICT

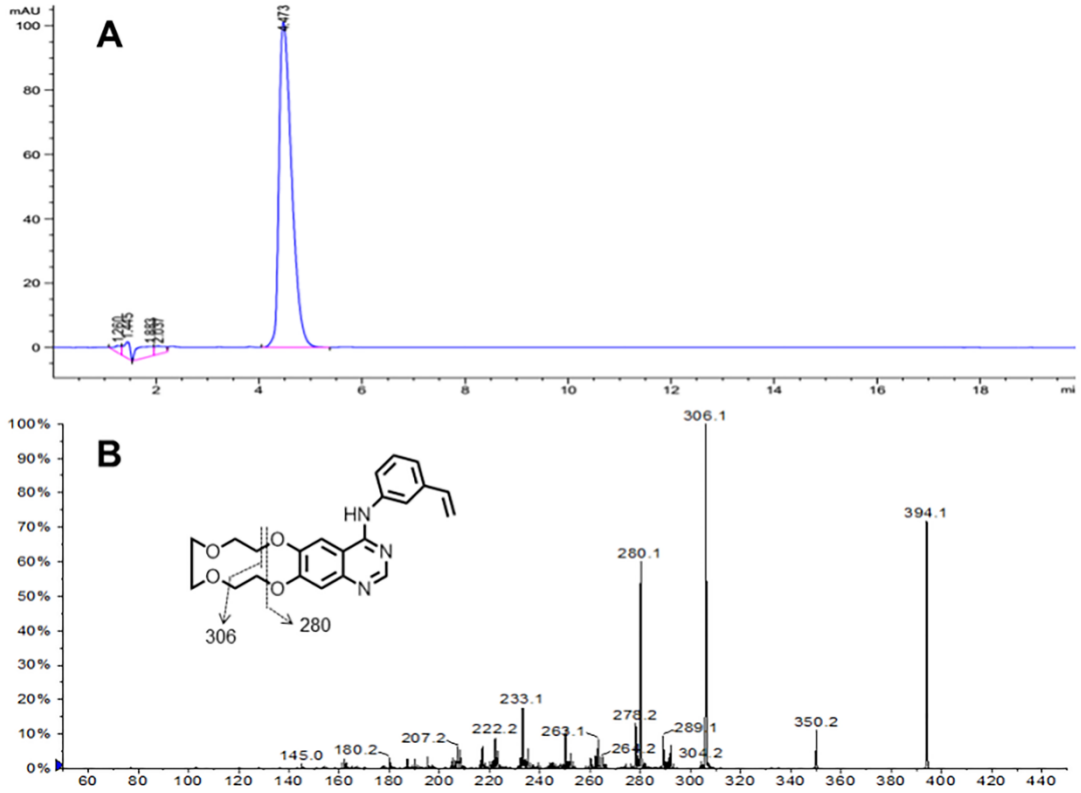

Supplemental Figure 4. HPLC-UV (A) and MS/MS (B) spectra of vinyl analog of ICT

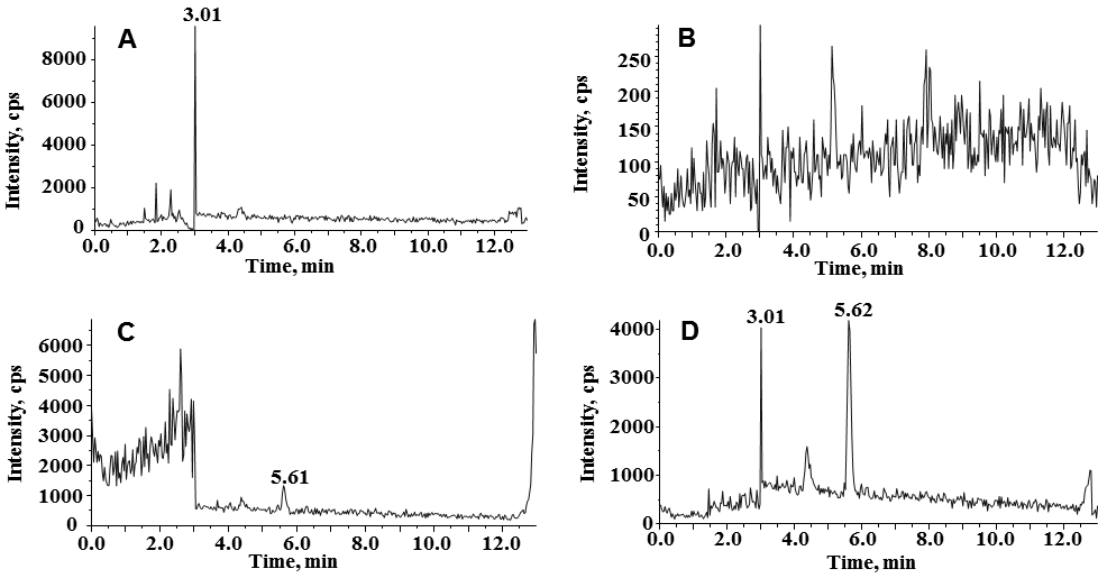

Supplemental Figure 5. Representative MRM chromatograms of 6*β*-hydroxytestosterone (A, C and D, *m/z* 305→269) and propranolol (B, *m/z* 261→116) obtained from analysis of boiled microsomal incubation mixtures lacking 6*β*-hydroxytestosterone and propranolol and of these spiked with 6*β*-hydroxytestosterone for the determination of LOD (2.5 ng/mL, C) or LLOQ (10 ng/mL, D)

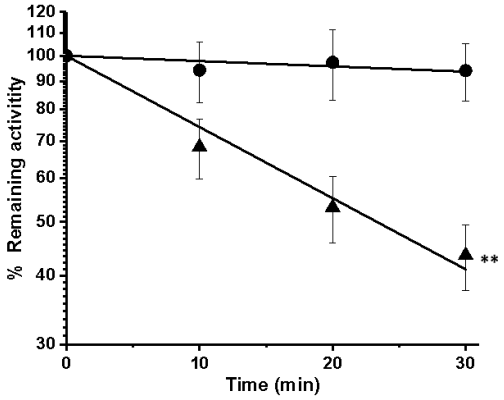

Supplemental Figure 6. Screening of time-dependent inhibition of CYP3A by ICT. NADPH-fortified human hepatic microsomes mixed with ICT at 0 (●) and 50 μM (▲) were incubated at 37 °C for various time periods and then submitted to enzyme activity measurement. Normalization was achieved by determination of enzymatic activity ratio at 0 min vs that of each time points. Data represent the mean ± SD (n = 3). * indicates the significance of the remaining enzyme activity of experimental groups in respect of that of control at the same time point (30 min) of incubations. Levels are considered significant at $^{**}p<0.01$.

$R_2 = (k_{obs} + k_{deg}) / k_{deg}$

Where $k_{obs} = (k_{inact} \times 50 \times I_{max,u}) / (K_{I,u} + 50 \times I_{max,u})$

k_{obs} is the observed (apparent first order) inactivation rate of the affected enzyme.
k_{deg} is the apparent first-order degradation rate constant of the affected enzyme.
$K_{I,u}$ is the unbound inhibitor concentration causing half-maximal inactivation.
k_{inact} is the maximal inactivation rate constant.
$I_{max,u}$ is the maximal unbound plasma concentration of the interacting drug at steady state.*

Note: I and K_I need to be expressed in the same unit (e.g., in a molar concentration unit).

*Considering uncertainties in the protein binding measurements, the unbound fraction in plasma should be set to 1% (fraction unbound in the plasma ($f_{u,p}$) = 0.01) if experimentally determined to be < 1%.

Supplemental Figure 7. Equations to calculate the R_2 value for basic models of time-dependent inhibition (FDA, 2020)